

Paula Faust Gouveia

**PHYSICOCHEMICAL AND BIOLOGICAL
CHARACTERIZATION OF BIOACTIVE GLASS/ZIRCONIA
BONE SUBSTITUTE MANUFACTURED BY THE REPLICA
METHOD**

Dissertação submetida ao Programa de Pós-Graduação em Ciência e Engenharia de Materiais da Universidade Federal de Santa Catarina como requisito para a obtenção do Título de Mestre em Ciência e Engenharia de Materiais.
Orientador: Prof. Dr.-Ing. Márcio Celso Fredel
Coorientador: Prof. Dr. Bruno A. P. C. Henriques

Florianópolis
2019

Ficha de identificação da obra elaborada pela autora através do
Programa de Geração Automática da Biblioteca Universitária da UFSC.

Gouveia, Paula

Physicochemical and biological characterization
of bioactive glass/zirconia bone substitute
manufactured by the replica method / Paula Gouveia
; orientador, Márcio Celso Fredel, coorientador,
Bruno A. P. C. Henriques, 2019.

92 p.

Dissertação (mestrado) - Universidade Federal de
Santa Catarina, Centro Tecnológico, Programa de Pós
Graduação em Ciência e Engenharia de Materiais,
Florianópolis, 2019.

Inclui referências.

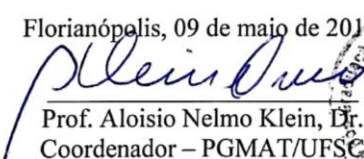
1. Ciência e Engenharia de Materiais. 2.
Biomateriais. 3. Regeneração Óssea. 4. Biocerâmicas.
5. Vidro Bioativo. I. Fredel, Márcio Celso. II. A.
P. C. Henriques, Bruno . III. Universidade Federal
de Santa Catarina. Programa de Pós-Graduação em
Ciência e Engenharia de Materiais. IV. Título.

Paula Faust Gouveia

**PHYSICOCHEMICAL AND BIOLOGICAL
CHARACTERIZATION OF BIOACTIVE GLASS/ZIRCONIA
BONE SUBSTITUTE MANUFACTURED BY THE REPLICA
METHOD**


Este Trabalho de Conclusão de Curso foi julgado adequado para
obtenção do Título de “Mestre em Ciência e Engenharia de Materiais” e
aprovado em sua forma final pelo
Programa de Pós-Graduação em Ciência e Engenharia de Materiais da
Universidade Federal de Santa Catarina.

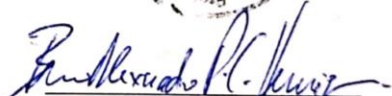
Florianópolis, 09 de maio de 2019

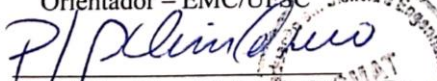

Prof. Aloisio Nelmo Klein, Dr.
Coordenador – PGMAT/UFSC

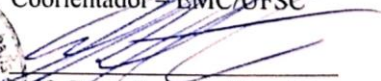


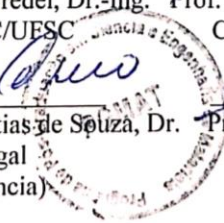
Banca Examinadora:


Prof. Márcio Celso Fredél, Dr.-Ing.
Orientador – EMC/UFSC


Prof. Bruno A. P.C. Henriques, Dr.
Coorientador – EMC/UFSC


Prof. Júlio César Matias de Souza, Dr.
CESPU/Portugal
(Videoconferência)


Prof. César Augusto Magalhães
Bênfatti, Dr. – Odonto/UFSC



Este trabalho é dedicado aos meus
pais: Norival Gouveia (*in memoriam*)
e Zaira C. F. Gouveia.

ACKNOWLEDGEMENTS

At first, I would like to thank both my advisor Prof. Dr.-Ing. Márcio Celso Fredel and co-advisor Prof. Dr. Bruno A. P. C. Henriques for the opportunity, support, guidance and transmitted knowledge, all so important throughout the entire process;

I also thank the Postgraduate Program in Materials Engineering (PGMAT), specially Rogério Antônio Campos e Prof. Dr. Guilherme Mariz de Oliveira Barra for always looking out for all students. Also, acknowledgments to CAPES for the financial support;

Dr. Joana Mesquita-Guimarães, for all the support provided;

MSc. Maria Elisa Galarraga, always so helpful, kind and warm;

My thanks to LCME, LEBm, LabMat labs and their collaborators;

To all my friends of CERMAT, Aldemir Luiz Dall-Astra, Elvira Lopes, Francesca Albino, Maria Ester Alfaro Cuervo, Rafael Vidal Eleutério, Roberta de Farias, Thaiane Balestreri Knopf and Thamyres Hellen da Silva, for always being so helpful and brightening even the dark days;

To a special friend I have found in this journey, Vivian Inês dos Santos, for always making things easier either by helping me or just laughing along;

To my sisters Beatriz Faust Gouveia, Fernanda Faust Gouveia and especially my mother Zaira Carlos Faust Gouveia, who always supports me and gives me the strength to carry on;

Finally, I have no words to thank George de Faria enough for his unconditional support and partnership for all these years.

I am thankful for every person that also contributed to this work and is not mentioned here.

Thank you!

RESUMO

O presente estudo apresenta uma rota para obtenção de arcabouços (*scaffolds*) compostos de vidro bioativo e zircônia para reparo ósseo, utilizando o método da réplica com esponjas de poliuretano (45, 60 e 80 ppi) como modelo. Os arcabouços são estruturas sintéticas ou naturais altamente porosas utilizadas no processo de cicatrização tecidual. Os materiais com propriedades bioativas, como o vidro bioativo 58S, são cada vez mais estudados e empregados para a confecção de arcabouços sintéticos. Um dos problemas com esses vidros bioativos é a sua baixa resistência mecânica, geralmente insuficiente durante o período de reparo ósseo. Dependendo da rota de obtenção, a resistência à compressão de arcabouços de vidro bioativo não superam 0,05 MPa. Desta forma, o objetivo principal deste estudo foi produzir arcabouços à base de vidro bioativo 58S e zircônia, utilizando o método da réplica. Para tal, foram obtidas estruturas porosas pré-sinterizadas (com *struts* ainda não completamente densificados) de zircônia que passaram por uma infiltração a vácuo com vidro bioativo 58S em estado sol-gel e só então foram sinterizadas a 1500 °C, formando assim uma estrutura que pode ser descrita como uma matriz de BG58S com partículas dispersas de zircônia. Seguidamente, os arcabouços de zircônia/BG foram recobertos com uma nova camada vidro bioativo (58S) em estado sol-gel e levado ao forno a 600 °C para sua consolidação. Arcabouços que não receberam o recobrimento após a sinterização também foram estudados a fim de conferir as propriedades bioativas resultantes do processo a elevadas temperaturas, bem como arcabouços compostos somente de zircônia para fins de comparação. Os resultados mostraram que a resistência à compressão dos *scaffolds* compostos pela combinação de BG e zircônia é similar às amostras de zircônia. Os ensaios *in vitro* mostraram a formação de HCAp nas amostras contendo BG58S, com maior intensidade na amostra onde o 58S foi tratado a 600 °C e, como esperado, menor nas amostras onde o vidro bioativo foi levado a altas temperaturas sem posterior recobrimento, o que mostra que as amostras mantiveram suas propriedades bioativas. Os testes de citocompatibilidade revelaram uma alta viabilidade celular em torno de 90% para *scaffolds* com infiltrações de BG58S. A infiltração nas estruturas pré-sinterizadas resulta em uma matriz de BG58S e a presença do vidro bioativo não influencia a resistência mecânica das estruturas. O tratamento térmico a 1500 °C não inibe totalmente a bioatividade desse

material, mas a prejudica, o que faz com que as amostras que receberam o segundo recobrimento com BG58S sejam as mais bioativas.

Palavras-chave: arcabouço, vidro bioativo, zircônia, bioatividade

ABSTRACT

The present study shows a manufacturing route of bioactive glass and zirconia scaffolds for bone repair, using the replica method with polyurethane sponges (45, 60 and 80 ppi) as a template. Scaffolds are highly porous synthetic or natural structures used for human tissue healing. Materials with bioactive properties, such as 58S bioactive glass, are increasingly being studied for scaffolds. One of the problems with these bioactive glasses is their poor mechanical strength, often not enough for applications in bone regeneration. Depending on the manufacturing method, the compressive strength of bioglass scaffolds do not achieve 0.05 MPa. Thus, the main objective of this study was to produce scaffolds based on 58S bioactive glass and zirconia, using the replica method. Scaffolds were obtained by pre-sintered porous structures of zirconia (with struts not yet completely densified) that underwent infiltration by sol-gel 58S bioactive glass under vacuum atmosphere and then sintered at 1500 °C. This process resulted in a structure which can be described as a BG58S matrix with dispersed zirconia particles. Afterwards, the zirconia/BG scaffolds were coated with a new layer of sol-gel BG58S and then submitted to a heat treatment at 600 °C for its consolidation. Scaffolds that did not receive the coating after sintering were also studied in order to check their bioactive properties resulted from the process at high temperatures. Both described scaffolds types were compared against structures composed only of zirconia, acting as reference material. Results revealed that there was no significant difference in compressive strength between BG58S/zirconia and zirconia scaffolds. The *in vitro* assays showed the formation of HCAp in both samples containing BG58S, with higher intensity in the scaffold which the BG58S was treated at 600 °C and, as expected, lower in the samples where the bioactive glass was brought to high temperatures without further coating, which evidences remaining bioactive properties. Cytocompatibility assays showed a cell viability at around 90% for BG58S/zirconia scaffolds. The BG58S infiltration on the pre-sintered scaffolds results in a glassy matrix and its presence does not influence the mechanical strength of the structure. Although after the heat treatment at 1500 °C the bioactivity of BG58S is still present, it is not the same, which makes the samples that received the final coating with BG58S the most bioactive.

Keywords: scaffolds, zirconia, bioactive glass, bioactivity, bone regeneration

LIST OF FIGURES

Figure 1 - Section of a bone illustrating the compact (dense) and the trabecular portions of the bone.....	27
Figure 2 - Crystalline phases of zirconia. From left to right: monoclinic, tetragonal and cubic.....	30
Figure 3 - Compositional dependence of bone and soft tissue bonding to bioactive glasses.....	32
Figure 4 - Flow diagram summarizing the steps involved in the determination of the route for obtaining zirconia reinforced bioactive glass scaffolds.	37
Figure 5 - Micrographs of the different types of scaffolds produced by different routes: monolithic zirconia (A and B); zirconia with BG coating (C and D); zirconia reinforced bioactive glass (E and F); zirconia reinforced bioactive glass with additional bioactive glass coating (G and H).	45
Figure 6 - Detailed view on the struts of the monolithic zirconia scaffolds (A), presenting a porous microstructure, and zirconia reinforced bioactive glass scaffolds (B), where a dense microstructure and a glassy matrix with dispersed zirconia particles can be seen.	46
Figure 7 - Zirconia scaffold sintered at 1200 °C and exhibiting insufficient strength denoted by the cracks and collapsed walls of the structure.....	46
Figure 8 - Cross-section view of a zirconia-reinforced bioactive glass scaffold (Group 3), showing the total infiltration of the BG58S in the zirconia pre-template. It is possible to observe that the BG fills all the void spaces inside each strut of the scaffold.....	47
Figure 9 - Typical depth-load hysteresis curves obtained from micro-indentation in the struts of the different groups of scaffolds.....	49

Figure 10 - Compressive strength of the monolithic zirconia scaffolds (G1); zirconia reinforced bioactive glass scaffolds: without bioglass coating (G3) and with bioactive glass coating (G4).50

Figure 11 - Micrographs of the scaffolds after 7 days of SBF soaking: A is the G1 sample, pure zirconia scaffold and presents no significant changes; B is a sample from G3, where the BG58S was submitted to 1500 °C with no further coating, it can be observed that there was a reaction on the surface with material deposition; and C the sample from G4 with BG58S coating up to only 600 °C showing a very typical hydroxyapatite structure.....51

Figure 12 - FEG micrograph of the hydroxyapatite layer with detailed spherical structure (10000x) on G4 scaffold after 7 days immersion in SBF. EDX analysis confirms the presence of Ca and P.52

Figure 13 - Schematic showing the bioactive glass coating in different substrates: A) monolithic zirconia substrate (G2), where the coating has a different CTE and composition from that of the substrate and, B) the substructure consists of a BG matrix with dispersed zirconia particles, which exhibits higher compositional and thermal compatibility to the BG coating.53

Figure 14 - Flow diagram summarizing the steps involved in obtaining bioactive glass hybrid scaffolds.....61

Figure 15 - Compressive strength of zirconia and bioactive glass hybrid scaffolds for 45, 60 and 80 ppi templates. The red and blue dots indicate the groups where significant statistical differences were found.....64

Figure 16 - Micrographs of the scaffolds after 12 h, 24 h, 72 h and 7 days of SBF soaking: Pure yttria-stabilized zirconia scaffolds do not present significant changes on its surface. After 7 days there are calcium-phosphate depositions on 1x 58S surface. The hybrid scaffolds 2x 58S present typical HCAp structures from 24 h of SBF with a thick HCAp layer after 7 days.66

Figure 17 - XRD patterns of samples after SBF immersion for 7 days. The red dots indicate characteristic peaks for HCAp crystal planes according to (JCPDS no. 09-0432). The blue triangles represent peaks for ZrO ₂ according to (JCPDS no. 14-0534) and 9486.....	67
Figure 18 - SEM image and EDX analysis of a 1x 58S scaffold after 4 weeks of SBF soaking. It is possible to observe Ca-P depositions along its surface.....	68
Figure 19 - SEM micrograph of a hybrid scaffold (2x 58S scaffold) after 4 weeks of SBF immersion. A thick HCAp layer is covering almost the entire surface of the sample.	69
Figure 20 - ZrO ₂ scaffold after 4 weeks of SBF immersion. For the EDX analysis, it can be concluded that these depositions are salt crystals and not calcium-phosphate structures.	69
Figure 21 - FTIR spectra of samples after 4 weeks of soaking in SBF. The red spot identifies the double peak characteristic of HCAp formation.	70
Figure 22 - SEM micrographs and EDS analysis of the Ca/P ratio on the 2x58S samples, before cell culture.	71
Figure 23 - a) Cell viability (by WST) results of MG-63 osteoblast-like cells on the uncoated and hybrid scaffolds after 7 days of cultivation. b) SEM image of the MG-63 osteoblast-like cells on the hybrid scaffolds 2x 58S after 7 days of cultivation in osteogenic medium.....	73

LIST OF TABLES

Table 1 - Some Applications of Biomaterials in Medicine	28
Table 2 - Properties of commercial zirconia powder TZ-3YSB-E... 38	
Table 3 - Summary of groups and processing routes.	40
Table 4 - Chemical composition of the SBF stock solution.	42
Table 5 - Density results obtained by the Archimedes method for groups G1, G3 and G4.....	48
Table 6 - Hardness (GPa) and Young's modulus (GPa) of the struts of the different scaffolds.....	49
Table 7 - Properties of commercial zirconia powder TZ-3YSB-E... 59	
Table 8 - Chemical composition of the SBF stock solution.	62
Table 9 - The pH of SBF following exposure to the scaffolds at given time points.	65
Table 10 - pH values of the samples immersed on DMEM solution after 48 and 96 hours of incubation.....	72

LIST OF ABBREVIATIONS

ppi – Pores Per Inches
HCAp – Hydroxy-carbonate apatite
PU – Polyurethane
CTE – Coefficient of Thermal Expansion
Y-TZP - Yttrium-stabilized Tetragonal Zirconia Polycrystal
G1 – Zirconia Scaffolds
G2 – Bioactive Glass 58S Coated Zirconia Scaffolds
G3 – Bioactive Glass 58S Infiltrated Zirconia Scaffolds
G4 – Bioactive Glass 58S Infiltrated and Coated Zirconia Scaffolds
SBF – Simulated Body Fluid
BG – Bioactive Glass
BG58S – Bioactive Glass 58S
TCP – Tricalcium phosphate
PLLA – Poly-L-lactic acid
G1 – Zirconia Scaffolds
G2 – Bioactive Glass 58S Coated Zirconia Scaffolds
G3 – Bioactive Glass 58S Infiltrated Zirconia Scaffolds
G4 – Bioactive Glass 58S Infiltrated and Coated Zirconia Scaffolds
RT – Room Temperature
SBF – Simulated Body Fluid
PP – Polypropylene
1x 58S – Bioactive Glass 58S Infiltrated Zirconia Scaffolds
2x 58S – Bioactive Glass 58S Infiltrated and Coated Zirconia Scaffolds

SUMMARY

1 INTRODUCTION.....	21
1.1 OBJECTIVES	22
1.1.1 General Objectives	22
1.1.2 Specific Objectives	22
1.2 STRUCTURE OF THE STUDY	22
2 LITERATURE REVIEW.....	25
2.1 BONE TISSUE	25
2.2 BIOMATERIALS	27
2.3 ZIRCONIUM DIOXIDE (ZIRCONIA).....	29
2.4 BIOACTIVE GLASS.....	31
2.5 SCAFFOLDS	33
3 ON THE OPTIMIZED PROCESSING ROUTE FOR THE PRODUCTION OF ZIRCONIA-REINFORCED BIOGLASS SCAFFOLDS FOR BONE REPAIR.....	35
3.1 INTRODUCTION.....	35
3.2 MATERIALS AND METHODS	38
3.3 RESULTS	43
3.4 DISCUSSION	52
3.5 CONCLUSIONS.....	55
4 IN-VITRO MECHANICAL AND BIOLOGICAL EVALUATION OF ZIRCONIA REINFORCED BIOACTIVE GLASS (58S) SCAFFOLDS FOR BONE REGENERATION.....	57
4.1 INTRODUCTION.....	57
4.2 MATERIALS AND METHODS	59
4.3 RESULTS	64
4.4 DISCUSSIONS.....	73
4.5 CONCLUSIONS.....	76

5	GENERAL CONCLUSIONS AND SUGGESTIONS.....	79
5.1	CONCLUSIONS	79
5.2	SUGGESTIONS	79
	REFERENCES	81

1 INTRODUCTION

The increased life expectancy that has been noted in the last years comes accompanied by a higher propensity to injuries in the human body. Whether it is in the field of medicine or dentistry, there is a growing need to find alternatives for the repair and regeneration of human body tissues, often damaged by trauma and diseases.

A major health-care issue is the bone defects resulting from tumours or traumas. There is a critical defect maximum size which the bone tissue can self-repair since it is a dynamic, highly vascularized tissue with a unique capability to heal and remodel. Thus, the autogenous healing can be compromised depending on the bone defect and therefore the use of graft materials is required to complete the repair of the tissue (CAPLAN; BRUDER, 2001).

The use of autogenous bone graft has considerable disadvantages such as limited source, donor morbidity, additional surgical procedures and, often, increased complex recovery. Although tissue can be harvested from a human donor, this alternative offers risks as disease transmission and adverse host immune response (HOLZWARTH; MA, 2012).

Engineering, especially Materials, often works in conjunction with medicine to find alternatives to increase life quality, by developing techniques for replacing or regenerating tissues and organs that have suffered damage. A great example are the bone implants (PEREIRA, 2011).

In order to repair this tissue, and not only provide replacement, scaffolds have been studied and produced aiming for the repair of trabecular bones and dental structures. To assist the regeneration of these tissues, materials that have bioactivity, such as bioactive glasses, are used. These materials have the capacity to bond to bone tissue, promoting osteoconduction and the proliferation of tissue cells.

One of the disadvantages of these materials is their low mechanical resistance, especially when used to fabricate highly porous structures (such as scaffolds). In some cases, bioactive glass scaffolds obtained by the replica method, using polyurethane sponges as sacrificial material, have such low mechanical strengths that these fall below the testing machine sensibility (<0.05 MPa) (BOCCARDI et al., 2016).

In order to overcome this problem, without losing porosity and affecting their function, scaffolds or porous implant structures are

produced from the combination of different materials. One example is the production of composite scaffolds, where there is a polymer matrix with dispersed bioactive glass particles.

Other proposals involve other materials, changes in the geometry and porosity of the scaffolds, as well as different routes for obtaining them.

In the present study, the possibility of reinforcing the 58S bioactive glass scaffolds with yttria-stabilized zirconia - a ceramic biomaterial already vastly studied and diffused in the dental and orthopedic area - was evaluated in order to increase its mechanical properties.

1.1 OBJECTIVES

1.1.1 General Objectives

To develop scaffolds composed by a 58S bioactive glass matrix reinforced with yttria-stabilized zirconia (3 mol%). The proposal is to create scaffolds that possess the bioactivity provided by the 58S at the same time as they offer satisfactory mechanical properties for practical applications.

1.1.2 Specific Objectives

- Define the best route for obtaining the scaffolds from the PU sponges;
- Evaluate the microstructure and mechanical properties of the new scaffolds, comparing with pure zirconia scaffolds;
- Investigate the bioactivity properties of the scaffolds;
- *In vitro* evaluation of biological behavior (cell viability).

1.2 STRUCTURE OF THE STUDY

This work is divided into five chapters. Chapter 1 consists of the present Introduction, where the objectives and motivations for such study are exposed.

Chapter 2 deals with a literature review, once the main goal is to provide a state of art on zirconia, bioactive glasses, scaffolds and implants.

In Chapter 3, an article focused on the optimization of the route to obtain bioactive glass scaffolds with mechanical resistance increased by adding a second ceramic phase is presented.

Chapter 4 englobes a second article, an extensive study of the behavior of the scaffolds obtained through the first article. Not only mechanical properties are evaluated here, but also biological characterization is performed.

At last, Chapter 5 showed an overview of the entire work with suggestions for further approaches and studies.

2 LITERATURE REVIEW

2.1 BONE TISSUE

The main component of the skeleton, bone tissue is a dynamic and multifunctional part of the human body that not only supports and protects soft tissues and vital organs, but it also plays roles in mineral homeostasis, hematopoiesis and performs an important endocrine function (BURR; ALLEN, 2014).

As a specialized type of connective tissue, human bone is a composite material, composed mainly by cells (osteocytes, osteoblasts and osteoclasts) that synthesize and regulates the extracellular matrix deposition and mineralization, modulating the complex mechanism of bone remodeling (JUNQUEIRA; CARNEIRO, 2013).

The mechanical functions of this tissue are performed by both trabecular and cortical bone, although each one plays a specific role. The dense cortical bone is responsible for supporting most of the load since it contains most of the bone mass. On the other hand, the porous trabecular bone may also play a role for load bearing, but one of its main functions is to redirect stresses to the stronger cortical shell (BURR; ALLEN, 2014).

The bone cells are described as follow:

- Osteocytes: flat cells that can be found inside the bone matrix, playing a vital role in its maintenance. Those type of cells can assist as a “stress sensor”, responding to mechanical stimulus and taking the information to the osteoblasts and osteoclasts that are responsible for bone remodeling. The matrix is reformulated in a way it can maintain the calcium homeostasis. (JUNQUEIRA; CARNEIRO, 2013; MARIEB; WILHELM; MALLATT, 2014).

- Osteoblasts: cells responsible for synthesizing the organic portion of bone matrix (Type I collagen, proteoglycans and glycoproteins) and playing a role on the matrix mineralization, since they have the capability of concentrating calcium phosphate. These cells can be found at the bone surface and once they become osteocyte since are surrounded by the newly formed matrix (JUNQUEIRA; CARNEIRO, 2013).

- Osteoclasts: giant, mobile, multinucleated cells responsible for bone tissue reabsorption. Osteoclasts secrete hydrochloric acid to dissolve the mineral component of the matrix and lysosomes to digest the organic components (JUNQUEIRA; CARNEIRO, 2013; MARIEB;

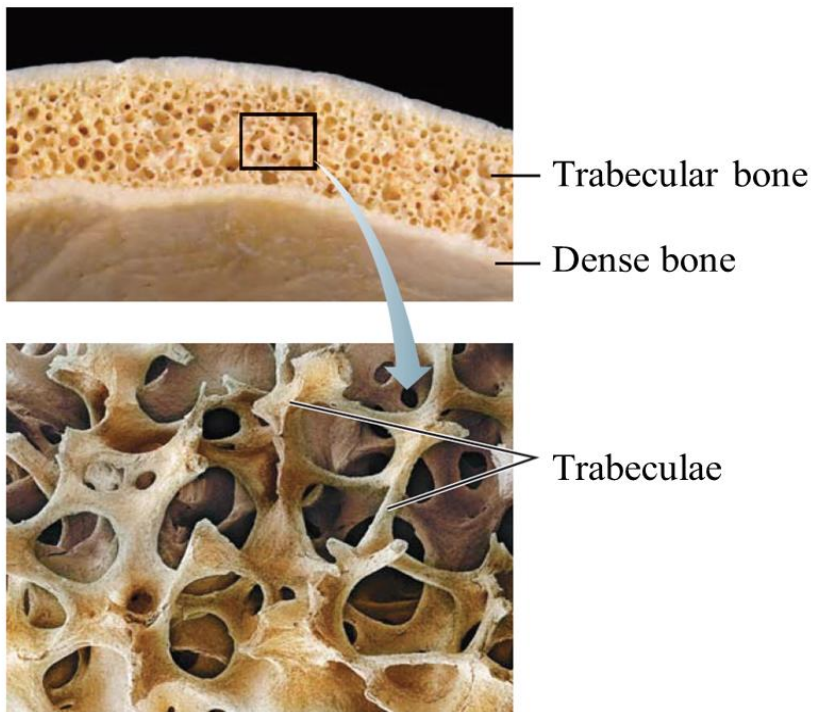
WILHELM; MALLATT, 2014). On dissolution of old bone tissue and replacing by a new one can maintain the strength and health of the bone on stresses (MARIEB; WILHELM; MALLATT, 2014).

The bone tissue is a specialized type of connective tissue of the human body that not only supports and protects soft tissues and vital organs, but it also plays roles in mineral homeostasis and hematopoiesis (BURR; ALLEN, 2014). The dense cortical bone is responsible for supporting most of the load since it contains a compact bone tissue. On the other hand, bone matrix is the extracellular mineralized part that contains numerous collagens fibers are embedded. Similar to other connective tissues (MARIEB; WILHELM; MALLATT, 2014). The porous trabecular bone tissue may also play a role on the transference of the stresses to the compact cortical shell (BURR; ALLEN, 2014).

The inorganic component of the matrix corresponds to 60-70% of its dry weight and contains mineral salts, mainly microcrystalline calcium and phosphate hydroxides, hydroxyapatite, (STANDRING et al., 2008) followed by small amount of bicarbonates, magnesium, potassium, sodium, and citrates (JUNQUEIRA; CARNEIRO, 2013). The inorganic constituents confer the hardness and stiffness of the bone (STANDRING et al., 2008). The organic portion of the matrix is mainly formed by collagen fibers (95%), proteoglycans, and glycoproteins (JUNQUEIRA; CARNEIRO, 2013). The organic components are responsible for ductility and tensile strength of the bone (MARIEB; WILHELM; MALLATT, 2014). (STANDRING et al., 2008).

Almost every bone presents a compact external layer that is macroscopically flat and solid, but when analyzed microscopically, passages for blood vessels and nerves can be identified. This layer is known as dense cortical bone. The spongy internal portion, the trabecular bone, with a “honeycomb” aspect is filled with red or yellow bone marrow (MARIEB; WILHELM; MALLATT, 2014). The difference between these parts is only macroscopic since they present the same histological base structure (JUNQUEIRA; CARNEIRO, 2013). Figure 1 shows a flat bone with a detailed vision of the cortical dense and the trabeculae structures.

Figure 1 - Section of a bone illustrating the compact (dense) and the trabecular portions of the bone.



Source: Adapted from (MARIEB; WILHELM; MALLATT, 2014)

2.2 BIOMATERIALS

According to the American National Institute of Health, biomaterials can be defined as “any substance or combination of substances, other than drugs, synthetic or natural in origin, which can be used for any period of time, which augments or replaces partially or totally any tissue, organ or function of the body, in order to maintain or improve the quality of life of the individual”.

Most biomaterials induct a non-specific, stereotyped biological response and that is why significant effort is dedicated to developing engineered surfaces that could induce rapid and precise reactions with cells and proteins. A complementary and important definition is that of “biocompatibility”: “Biocompatibility is the ability of a material to

perform with an appropriate host response in a specific application (Williams, 1987)” (RATNER et al., 2013).

Examples of “appropriate host responses” can be resistance to blood clotting, resistance to bacterial colonization, and normal, uncomplicated healing. Examples of specific applications can be seen in Table 1 and it is notable that some of the applications can be in contact with the patient body for hours (hemodialysis membrane for example), a week (catheter) or a lifetime of the patient, like a hip joint for example (RATNER et al., 2013)

Table 1 - Some Applications of Biomaterials in Medicine

Application	Types of materials
Skeletal system	
Joint replacements (hip, knee)	Titanium, Ti-Al-V alloy, stainless steel, polyethylene
Bone plate for fracture fixation	Stainless steel, cobalt-chromium alloy
Bone cement	Poly(methyl methacrylate)
Bony defect repair	Hydroxylapatite
Artificial tendon and ligament	Teflon, Dacron
Dental implant for tooth fixation	Titanium, Ti-Al-V alloy, stainless steel, polyethylene Titanium, alumina, calcium phosphate
Cardiovascular system	
Blood vessel prosthesis	Dacron, Teflon, polyurethane
Heart valve	Reprocessed tissue, stainless steel, carbon
Catheter	Silicone rubber, Teflon, polyurethane
Organs	
Artificial heart	Polyurethane
Skin repair template	Silicone-collagen composite
Artificial kidney (hemodialyzer)	Cellulose, polyacrylonitrile
Heart-lung machine	Silicone rubber
Senses	
Cochlear replacement	Platinum electrodes
Intraocular lens	Poly(methyl methacrylate), silicone rubber, hydrogel
Contact lens	Silicone-acrylate, hydrogel
Corneal bandage	Collagen, hydrogel

Source: (RATNER et al., 2013)

Osseointegration is critical for the implant stability, and it can be defined as a direct structural and functional connection between the living bone and the surface of the implant with no interposition of non-

bone tissue, such as fibrous or connective tissue (MAVROGENIS et al., 2009; PARITHIMARKALAIIGNAN; PADMANABHAN, 2013). This process depends not only on the biocompatibility of the material but also on the alteration of the mechanical environment. It starts with an initial interlocking between bone and the implant with subsequent biological fixation through continuous bone apposition and remodeling (PARITHIMARKALAIIGNAN; PADMANABHAN, 2013).

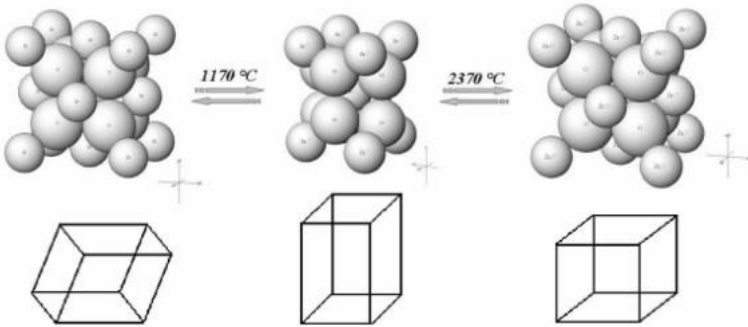
Bone ingrowth takes place inside a porous surface and for that to happen pores size must be from 50 to 400 μm . Also, the percentage of voids within the coating should be between 30% and 40% to maintain mechanical strength (KHANUJA et al., 2011). While pore shape does not influence the growth rate, the pores size and its interconnectivity play a major role on the cell migration, cell adhesion, and angiogenesis (RATNER et al., 2013).

Nowadays, an implant is considered to be osseointegrated when there is no relative progressive movement relative to the bone (MAVROGENIS et al., 2009) and it is a prerequisite for implant loading and long-term success (PARITHIMARKALAIIGNAN; PADMANABHAN, 2013).

2.3 ZIRCONIUM DIOXIDE (ZIRCONIA)

Zirconium dioxide (ZrO_2), also known as zirconia, is a ceramic material that presents three polymorphs, which means it has three distinctive crystalline phases. As shown in Figure 2, on temperatures under 1170 $^\circ\text{C}$, it exhibits the monoclinic form. Between 1170 $^\circ\text{C}$ and 2370 $^\circ\text{C}$ it presents the tetragonal form and above that temperature, it is found on the cubic phase until its melting point around 2680 $^\circ\text{C}$ (SANTOS, 2012).

Figure 2 - Crystalline phases of zirconia. From left to right: monoclinic, tetragonal and cubic.



Source: (BIRRER, 2009).

Zirconia is an extremely refractory material, with low thermal conductivity, high mechanical, chemical and high temperatures corrosion resistance. Along with other properties such as high density, high wear resistance and fracture toughness, zirconia is suitable for applications in various fields: cutting tools, dental crowns, medical implants, fuel cells, jewelry (Gouveia 2016; C. Dos Santos and Elias).

Transition from monoclinic to tetragonal structure

The martensitic monoclinic to tetragonal transformation has a positive (toughening transformation) and a negative consequence (low-temperature degradation, microcracking). (DEVILLE; GUÉNIN; CHEVALIER, 2004) This negative characteristic is due to a volume variation of approximately 4.5% (SANTOS, 2012), which makes pure zirconia not suitable for most applications, prosthetic components for example (DOS SANTOS; ELIAS; FABRIS; PAXTON; FINNIS, 2002).

To overcome this problem, low valence oxides such as calcium oxide (CaO), magnesium oxide (MgO), cerium oxide (CeO₂) or yttrium oxide (Y₂O₃) are added to disadvantage the monoclinic phase and stabilize the phases with more symmetrical structures: tetragonal and cubic (DEVILLE; GUÉNIN; CHEVALIER, 2004; FABRIS; PAXTON; FINNIS, 2002).

Yttria-stabilized tetragonal zirconia polycrystal (Y-TZP)

As the concentration of dopant (oxide) increases, the material takes the tetragonal phase and it is called partially stabilized. Then, when it maintains the cubic phase, it is called fully stabilized. The

amount of dopant required to achieve such stabilization in the cubic phase is relatively high - not less than 8 mol% of Y_2O_3 to achieve total stabilization (FABRIS; PAXTON; FINNIS, 2002).

By adding small concentrations of yttria (around 2 to 5% mol) to pure zirconia, it is possible to obtain up to 98% of the metastable tetragonal phase. The material is then suitable for various applications, including medical, due to the excellent physical, mechanical and thermal properties. (SANTOS, 2012)

Besides the high mechanical resistance, fracture toughness, high hardness, wear resistance and non-magnetic behavior, yttria-stabilized zirconia is also a good electrical and thermal insulator, with Young's modulus close to the stainless steel and thermal expansion coefficient similar to iron. (SANTOS, 2012)

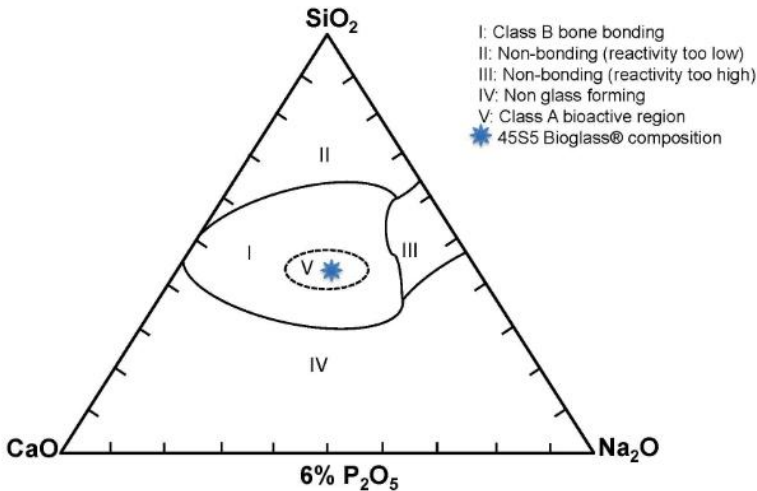
2.4 BIOACTIVE GLASS

Bioactive glasses are synthetic biomaterials known for their capability of stimulating bone healing when in contact with this tissue. They can be defined as glasses designed to obtain a specific biological response through controlled reactions on its surface. (ORÉFICE, R. L.; PEREIRA, M. D. M.; MANSUR, 2006)

The first bioactive glass composed of 46.1 mol% SiO_2 , 24.4 mol% Na_2O , 26.9 mol% CaO and 2.6 mol% P_2O_5 was developed by Larry Hench, in 1969, an assistant professor at the University of Florida. It was later known as Bioglass 45S5, a glass capable of forming a chemical bond with bone tissue. (JONES, 2012; L.L. HENCH, R.J. SPLINTER, W.C. ALLEN, 1972)

The following diagram (Figure 3) illustrates the capability of bioactive glasses to establish a bond with bone tissue depending on the chemical composition ranging from 45 up to 55% mol of SiO_2 . The chemical composition of Bioglass 45S5 is represented at the region V in the Figure 3.

Figure 3 - Compositional dependence of bone and soft tissue bonding to bioactive glasses.



Source: (HENCH, 2015).

The bioactivity of these glasses is related to the formation of a hydroxyapatite layer on its surface with composition and structure similar to those of the mineral part of the bone tissue (HENCH, 1991). This process occurs through ions exchange between the glass and the medium around. In general, the more amorphous the material, the greater its reactivity and ease in exchanging these ions to generate the hydroxyapatite layer.

It was found that when bioactive glass crystallizes (for example, due to high processing temperatures), the degree of bioactivity decreases when compared to the amorphous material (MA et al., 2010).

Bioactive glass 58S

Although Bioglass 45S5 is the most widely used and studied, it has some practical disadvantages. It is obtained by the casting process, which results in very high synthesis temperatures. To overcome this problem, in the 1990s, a new bioactive glass was developed: 58S bioactive glass, with the following composition: 60% SiO₂, 36% CaO, 4% P₂O₅ (% mol) and 58% SiO₂, 33% CaO, 9 % P₂O₅ (% by weight), obtained by the sol-gel process (HOPPE, A.; GÜLDAL, N. S.; BOCCACCINI, 2011; SEPULVEDA, P.; JONES, J. R.; HENCH, 2001; ZHONG, J.; GREENSPAN, 2000).

Through this process, it is possible to obtain a bioactive glass with composition and biological properties like the ones of the BG45S5, with lower processing temperatures – from room temperature to about 600 °C.

2.5 SCAFFOLDS

Scaffolds are highly porous structures used in tissue engineering, which can be implanted into bone defects to repair the tissue through adhesion, growth and proliferation of new cells in this structure (PEREZ RA, 2016; SHADJOU N, 2015).

The main role of the scaffold, in the case of bone, is to act as a 3D support for tissue healing. The design of highly porous scaffolds is often critical. It must possess proper morphological and functional properties to induce cell adhesion, differentiation and proliferation, with adequate mechanical integrity to maintain the original and desirable structure, non-cytotoxicity, and osteoconductivity, acting as a synthetic and temporary extracellular matrix (MA, 2004a; WANG et al., 2007).

The success of the scaffolds is due to their high porosity and interconnected pore network design, that can facilitate cell seeding, nutrient supply and metabolic waste removal, which accelerates bone regeneration (LAURENCIN; KHAN; EL-AMIN, 2006).

A bioactive porous material or scaffold should reveal enhanced 3D porous design (pores ranging from 300-500 μm), bioactivity, osteoconductivity, angiogenesis potential, biodegradability, and mechanical strength (DO VALE PEREIRA, 2011; HING, 2005; HUTMACHER, 2000; LAURENCIN; KHAN; EL-AMIN, 2006; LOH; CHOONG, 2013; MOHAMAD; BRETCANU; BOCCACCINI, 2008; REZWAN et al., 2006; TIAINEN et al., 2010).

3 ON THE OPTIMIZED PROCESSING ROUTE FOR THE PRODUCTION OF ZIRCONIA-REINFORCED BIOGLASS SCAFFOLDS FOR BONE REPAIR

3.1 INTRODUCTION

Scaffolds are highly porous structures used in tissue engineering that can be implanted in bone defects to promote its regeneration through adhesion, growth and proliferation of new cells in this structure (PEREZ RA, 2016; SHADJOU N, 2015).

The main role of this structure is to serve as a substrate for this cell adhesion, guiding the proliferation and differentiation of the cells so they will form the bone tissue to repair the injury as the scaffold is degraded by the organism (DO VALE PEREIRA, 2011).

For a scaffold to be successful, it must display the following characteristics: biocompatibility, osteoconductivity, mechanical properties compatible to the ones of the tissue and enough porosity so the cells can migrate in all directions, promote tissue growth and vascularization (DO VALE PEREIRA, 2011; HING, 2005; HUTMACHER, 2000; LOH; CHOONG, 2013; MOHAMAD; BRETCANU; BOCCACCINI, 2008; REZWAN et al., 2006; TIAINEN et al., 2010).

The material used to produce the scaffold must have high biocompatibility and induce bone cell attachment and differentiation in order to promote a direct bone-to-scaffold interface (JONES; HENCH, 2003; KARAGEORGIU; KAPLAN, 2005; SAIZ et al., 2013). Bioceramics are strongly used for bone tissue engineering due to their chemical and structural similarity to the mineral part of the native bone (BELLUCCI; CANNILLO; SOLA, 2012; SEBDANI; FATHI, 2011).

Bioactive glasses are biomaterials known for the capacity of stimulating bone repair when in direct contact with the tissue. It can be defined as glasses designed to obtain a specific biological response through controlled reactions of their surface (ORÉFICE, R. L.; PEREIRA, M. D. M.; MANSUR, 2006).

Their bioactivity is related with the formation of a hydroxyl-carbonate apatite (HCAp) layer on its surface with structure and composition similar to the mineral part of the bone tissue, resulting on a biological match between the material and bone tissues (HENCH, 2015; JONES, 2015). Such process occurs due to ions exchange between the glass and the medium where it is located. In general, the more

amorphous the material, the greater its reactivity and ease in exchanging these ions and promoting the formation of the hydroxyapatite layer (MA et al., 2010).

The first bioactive glass was the Bioglass 45S5 invented in 1969 by Larry Hench when observing the bond between a silicate-based glass and rat bones (JONES, 2015; L.L. HENCH, R.J. SPLINTER, W.C. ALLEN, 1972; RAHAMAN et al., 2012). It is still the most used and studied, but it presents a few practical disadvantages, such as its extremely high processing temperatures. To overcome this problem, in the 1990s, a new bioactive glass was developed, the 58S, with the following composition: 60%SiO₂, 36%CaO, 4% P₂O₅ (% mol) and 58%SiO₂, 33%CaO, 9%P₂O₅ (% wt), obtained by sol-gel process (HOPPE, A.; GÜLDAL, N. S.; BOCCACCINI, 2011; SEPULVEDA, P.; JONES, J. R.; HENCH, 2001; ZHONG, J.; GREENSPAN, 2000). Sepulveda et al. (SEPULVEDA; JONES; HENCH, 2002a) showed that 58S gel-glass powders present even higher dissolution rates for apatite formation when compared to melt-derived 45S5 glass powders. The sol-gel process provides a bioactive glass with composition and biological properties close to those of Bioglass 45S5 but with lower processing temperatures (from room temperature to 600 °C).

One important disadvantage of these materials is their very low fracture toughness (FU et al., 2011) and strength, especially when used to obtain highly porous structures such as scaffolds. The compressive strength typically reported in the literature for bioglass scaffolds obtained through replica method with polyurethane as the sacrificial template hardly exceeds 0.05 MPa (BOCCARDI et al., 2016; HUM; BOCCACCINI, 2018).

In order to enhance the mechanical resistance without changing the geometry or porosity of the scaffold, which can affect its function, composite scaffolds with a polymeric matrix are being studied (DO VALE PEREIRA, 2011). Another alternative that has been pursued is to coat a ceramic scaffold with a bioactive glass (by the dipping the ceramic scaffold in a bioactive glass powder suspension), which can be hindered by delamination occurrences due to the Coefficients of Thermal Expansion (CTE) mismatch between both materials. Silicate-based bioactive glasses typically possess CTE ranging between $12-16 \times 10^{-6}/^{\circ}\text{C}$, while ceramics such as zirconia and alumina, highly used in biomedical applications, present CTE around $10.5 \times 10^{-6}/^{\circ}\text{C}$ and $8 \times 10^{-6}/^{\circ}\text{C}$, respectively. A high CTE value of the coating can place the coating in tension, which further weakens the bioglass layer (GOMEZ-VEGA et al., 2000; LACEFIELD; HENCH, 1985; SCHUBERT, 1986).

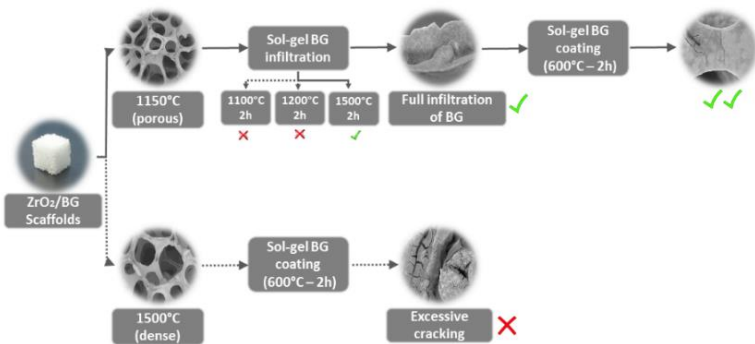
That is the reason why different bioactive glasses compositions are being tested, for example, to achieve CTE closer to the one of the chosen ceramic material (ZHANG; LEGEROS; KIM, 2014). The focus of this work was to produce bioactive glass scaffolds with a second ceramic phase to enhance its mechanical resistance.

Yttria-stabilized zirconia (Y-TZP) presents excellent mechanical properties such as high fracture toughness combined with biocompatibility, which is why it has been increasingly used in the biomedical and dental field (CHEVALIER, 2006; DENRY; KELLY, 2008; GOUVEIA et al., 2017; ÖZKURT; KAZAZOĞLU, 2011). This oxide ceramic is used in orthopedic prostheses and dental implants since it is very suitable for applications where high strength and fracture toughness are required (CHEVALIER, 2006; KELLY; DENRY, 2008).

Therefore, this work aimed to investigate a processing route to obtain zirconia reinforced bioactive glass scaffolds, through the replica method. We were able to produce bioactive scaffolds, containing zirconia reinforcing particles within a bioactive glassy matrix, allowing to enhance scaffolds strength without compromising its bioactive characteristics.

As it is going to be shown along with this work, Figure 4 resumes the attempts made to obtain the expected results, highlighting the successful processes and parameters.

Figure 4 - Flow diagram summarizing the steps involved in the determination of the route for obtaining zirconia reinforced bioactive glass scaffolds.



Source: Author.

3.2 MATERIALS AND METHODS

Ceramic powder

For this study, yttria-stabilized zirconia spray-dried powder (TZ-3YSB-E, TOSOH Co., Tokyo, Japan) with high purity (99% ZrO₂) and properties according to Table 2 was used. According to the supplier, the powder has a maximum particle size of 120 μm and spherical agglomerates with an average size of 60 μm.

Table 2 - Properties of commercial zirconia powder TZ-3YSB-E.

Density (g/cm³)	6.05
Green density (g/cm³)	2.79
Hardness (HV10)	1250
Bending strength (MPa)	1100
Fracture toughness (MPa*m^{1/2})	5

Source: Tosoh Co.

Ceramic suspension

The zirconia suspension was prepared according to the method described elsewhere (MESQUITA-GUIMARÃES et al.). Suspensions thus contained 60 wt% of yttria-stabilized zirconia powder and 1 wt% of Duramax D3005, a dispersant used to adjust the pseudoplastic and thixotropic rheological behavior. (MESQUITA-GUIMARÃES et al.)

The suspension was obtained by adding 20 ml of distilled water to 30 g of zirconia powder. It was then milled in a planetary ball mill (PM100, Retsch) for 80 min at 400 rpm for powder deagglomeration and slurry homogenization. Afterward, the dispersant Duramax was added to achieve the desired rheological behavior.

Bioactive glass 58S

The 58S bioactive glass (BG58S) (58 wt % SiO₂, 33 wt % CaO, 9 wt % P₂O₅) was synthesized by the sol-gel method (GALARRAGA-VINUEZA et al., 2017b). An alternative sol-gel synthesis was used when compared with others already reported (PEREIRA et al., 2014). Tetraethyl Orthosilicate (TEOS) (98%, Sigma–Aldrich, USA), triethyl phosphate (TEP) (99.8%, Sigma–Aldrich, USA) and calcium nitrate tetrahydrate (Ca(NO₃)₂·4H₂O) (Vetec, Brazil) were used as precursors of silicon, phosphorous and calcium oxide, respectively. Ethyl alcohol (EtOH, P.A., Synth, Brazil) was used as solvent of TEOS and TEP, and nitric acid (HNO₃, 68%, Vetec, Brazil) was used to

dissolve $\text{Ca}(\text{NO}_3)_2 \cdot 4\text{H}_2\text{O}$, respecting the “like dissolves like” chemical dissolution rule (BETTELHEIM et al., 2009).

First of all, to do the synthesis, the molar ratio of SiO_2 , P_2O_5 , and CaO were calculated respecting weight amounts of the 58S. Then, TEOS was added to EtOH in a glass beaker under magnetic stirring. The beaker was covered with paraffin film to avoid evaporation and then stirred for 10 min. TEP was added to this solution in constant agitation and stirred for 10 min. $\text{Ca}(\text{NO}_3)_2 \cdot 4\text{H}_2\text{O}$ was dissolved in 2M HNO_3 and added to water at a molar ratio TEOS: H_2O of 1:4. This mixture was added to the solution and stirred for 1 h. During solution preparation, heating was avoided to prevent solvent evaporation.

Polyurethane sponges

To serve as sacrificial templates at the replica method, polyurethane (PU) sponges of 60 pores per inch (ppi) were cut into 1 cm^3 cubes (10 mm x 10 mm x 10 mm).

Scaffolds production processes

For the development of the best combination of route and results, four groups of scaffolds were selected and for each group, 20 samples were produced using PU sponges of 60 ppi as sacrificial templates.

The first group (G1) is the control group and contains only zirconia (TZ-3YSB-E) in its composition. This group is important to assess whether the strength of the new zirconia reinforced scaffolds will be higher or lower than the reference. Additionally, it works as a negative group for *in vitro* assays, since it is expected to have no bioactive properties.

The PU sponges were manually impregnated with the ceramic suspension without clogging the pores and kept in a stove at 100 °C for 20 min. A heat treatment with the usual parameters for sintering this material (1500 °C at 5 °C/min for 120 min) was performed in a conventional high-temperature furnace to eliminate PU and consolidate the scaffolds. At the end of the treatment, fully sintered monolithic Y-TZP scaffolds were obtained.

The second group (G2) of samples includes a BG58S coating on the zirconia scaffolds. It is important in terms of comparison to observe how this coating would behave, especially in terms of its adhesion to the substructure. Hence, for the production of G2 samples, scaffolds equal to those of the G1 group (fully sintered scaffolds) were dipped in BG58S solution at a glass beaker, which was then placed inside a

vacuum chamber for 10 min. Afterward, samples were subjected to a heat treatment at 600 °C for consolidation of the bioactive glass.

The third group (G3) includes an additional step before the sintering heat treatment of the zirconia scaffolds. For that, after PU sponges had been impregnated with zirconia suspension and placed in a stove for 20 min at 100 °C, a heat treatment at 1150 °C at 1 °C/min for 120 min was performed to eliminate the PU sponge and pre-consolidate the scaffold. The result was a template of a zirconia scaffold that was porous (not fully sintered) but with adequate strength to be handled. The zirconia templates were then dipped in a BG58S sol-gel solution (same as described before) and went for vacuum chamber for 10 min after which they were sintered at 1500 °C at 5 °C/min for 120 min (the typical sintering procedure used for zirconia). Lower sintering temperatures for these scaffolds, such as 1100 °C and 1200 °C, were tested but without success. The scaffolds did not exhibit adequate strength, breaking while handling. These lower sintering temperatures were tested because they should possibly be less harmful to bioactive glass.

Finally, the fourth group (G4) consisted of the same samples as those of the third group (G3) that received an additional BG58S coating. Hence, the samples produced in similar conditions of the G3 samples were placed in a vacuum chamber for 10 min, and afterward heat-treated at 600 °C for 120 min at 1 °C/min. Table 3 resumes the groups of samples and their respective processing routes.

Table 3 - Summary of groups and processing routes.

G1	ZrO ₂	Pure ZrO ₂ (Control Group)		
G2	C/ZrO ₂	ZrO ₂ template; 1500 °C; 2 h	→	Sol-gel BG coating; 600 °C; 2 h
G3	INF/ZrO ₂	ZrO ₂ template; 1150 °C; 2 h	→	Sol-gel BG coating; 1500 °C; 2 h
G4	C/INF/ZrO ₂	ZrO ₂ template; 1150 °C; 2 h	→	Sol-gel BG coating; 1500 °C; 2 h
				→ Sol-gel BG coating; 600 °C; 2 h

Source: Author.

Microstructure analysis

A qualitative analysis of the microstructure of the scaffolds was performed using a Scanning Electron Microscope coupled with energy dispersive X-ray spectroscopy (TM3030 Hitachi, Japan) to observe the adherence and homogeneity of the bioactive glass coatings.

Density

The density of the sintered scaffolds was determined using an Archimedes device, precision balance and was calculated using Eq. (1):

$$SD = \frac{W1 \times WDT}{W4 - W2} \quad (1)$$

W1: Weight of sintered body at room temperature.

W2: Keep the sintered body in boiling water for one hour. After cooled down to room temperature (R.T.), the weight (W2) is measured in the water at R.T.

W4: After removing water from the surface, weight (W4) of the sintered body is measured.

WDT: density of water at T °C.

The porosity p was then calculated by

$$p(\%) = \left(1 - \frac{\rho_{foam}}{\rho_{solid}}\right) \cdot 100 \quad (2)$$

where $\rho_{solid} = 6.05 \text{ g/cm}^3$ for group G1 and $\rho_{solid} = 5.57 \text{ g/cm}^3$ for groups G3 and G4. The latter density was computed using the rule of mixtures considering the content of each phase in the microstructure (77% of zirconia and 33% of 58S Bioactive glass). The density of 58S bioactive glass was taken as 2.7 g/cm^3 (SEPULVEDA, P.; JONES, J. R.; HENCH, 2001).

Micro-indentation test

Micro-indentation test was conducted on G1, G3 and G4 scaffolds in order to evaluate the mechanical properties of the struts. The samples were embedded in resin and polished to perform the test. A micro/nano-indenter (NanoTest, Micro Material Limited, Wrexham, UK) equipped with a diamond indenter with Berkovich pyramidal tip (100 nm diameter) was used. Load-depth curves were recorded using a maximum load up to 500 mN and load rate of $5 \mu\text{N/s}$. For Young's Modulus determination, we have taken the reduced modulus, given the big difference in relation to that of the diamond indenter.

Mechanical characterization

Compressive strength tests were carried out in a universal testing machine (23-5S, INSTRON/EMIC, Brazil – LEBm UFSC) with a 50 N load cell and 1 mm/min test rate. The tests were performed until 25% of the total height of the samples (JAIN et al., 2003; MESQUITA-GUIMARÃES et al., 2017). A total of 10 samples of each condition was tested.

Statistical analysis

The results were analyzed using one-way ANOVA followed by Tukey's test. The Kolmogorov_Smirnov test was first applied to test the assumption of normality. Differences between the group's compressive strength were tested using t-test. P values lower than 0.05 were considered statistically significant.

In vitro apatite-forming assay

Simulated body fluid (SBF) was obtained according to Kokubo's method and its chemical composition can be seen in Table 4 (KOKUBO; TAKADAMA, 2006). Samples from G1, G3 and G4 were immersed into 30 mL of SBF solution in sterilized PP tubes. The tubes were stored in an incubator at 37 °C for 7 days. Each sample was run in triplicate and after the period they were removed from the solution, washed with deionized water and dried in an oven at 37 °C for 24 h.

The capability of forming a hydroxyapatite layer on the surface of the samples was evaluated by Scanning Electron Microscope (SEM) with Energy Dispersive X-Ray Spectroscopy (EDX) and Field Emission Gun Scanning Electron Microscope (JEOL JSM-6701F (FEG) LCME - UFSC).

Table 4 - Chemical composition of the SBF stock solution.

Order	Reagent	Amount
1	NaCl	8.035 g
2	NaHCO ₃	0.355 g
3	KCl	0.225 g
4	K ₂ HPO ₄ · 3H ₂ O	0.231 g
5	MgCl ₂ · 6H ₂ O	0.311 g
6	1.0 _M - HCl	39 mL
7	CaCl ₂	0.292 g
8	Na ₂ SO ₄	0.072 g
9	Tris	6.118 g
10	1.0 _M - HCl	0 – 5 mL

Source: Adapted from (KOKUBO; TAKADAMA, 2006)

3.3 RESULTS

Microstructure analysis

Figure 5 shows the micrographs of the samples from G1 to G4 groups. Figure 5A and B show a general and detailed view, respectively, of the scaffolds from the control group (G1) made of monolithic zirconia. It can be seen from Figure 5A that the sponge format has been reproduced without significant defects in the struts. The higher magnification view depicted in Figure 5B further confirms the defectless struts and shows that struts are porous at their surface and bulk. The sharp edges throughout the scaffold can also be noticed and evidence a characteristic of this type of scaffold.

Figure 5C and D show the micrographs of the monolithic zirconia scaffolds with a 58S bioactive glass coating. It is possible to observe that the bioactive glass coating presents high irregularity and is not homogeneously distributed over the surface of the strut. Additionally, at the accumulation regions, the BG tended to crack which impart lower cohesion to the coating and also lower adhesion to the zirconia substructure, favoring delamination occurrences. In these scaffolds, no infiltration of the bioglass in the zirconia struts was noticed. Hence, a new strategy was employed for groups G3 and G4, consisting in using pre-sintered zirconia templates of higher porosity that could thus be infiltrated by the bioactive glass in sol-gel solution.

The micrographs of the novel zirconia reinforced bioactive glass scaffolds (G3) are presented in Figure 5E and F. In these scaffolds, a porous pre-template of zirconia has been created and then infiltrated with bioactive glass 58S in sol-gel solution. The consolidation of the whole structure was afterward achieved during the sintering treatment of zirconia. The result of such process is evidenced by scaffolds with more organic and smoother shapes (Figure 6B), contrasting to those exhibited by G1 scaffolds and seen in Figure 5A, Figure 5B and Figure 6A. The microstructure of these scaffolds is also different from Groups 1 and 2, consisting of a bioglass matrix with dispersed zirconia particles as depicted in Figure 6.

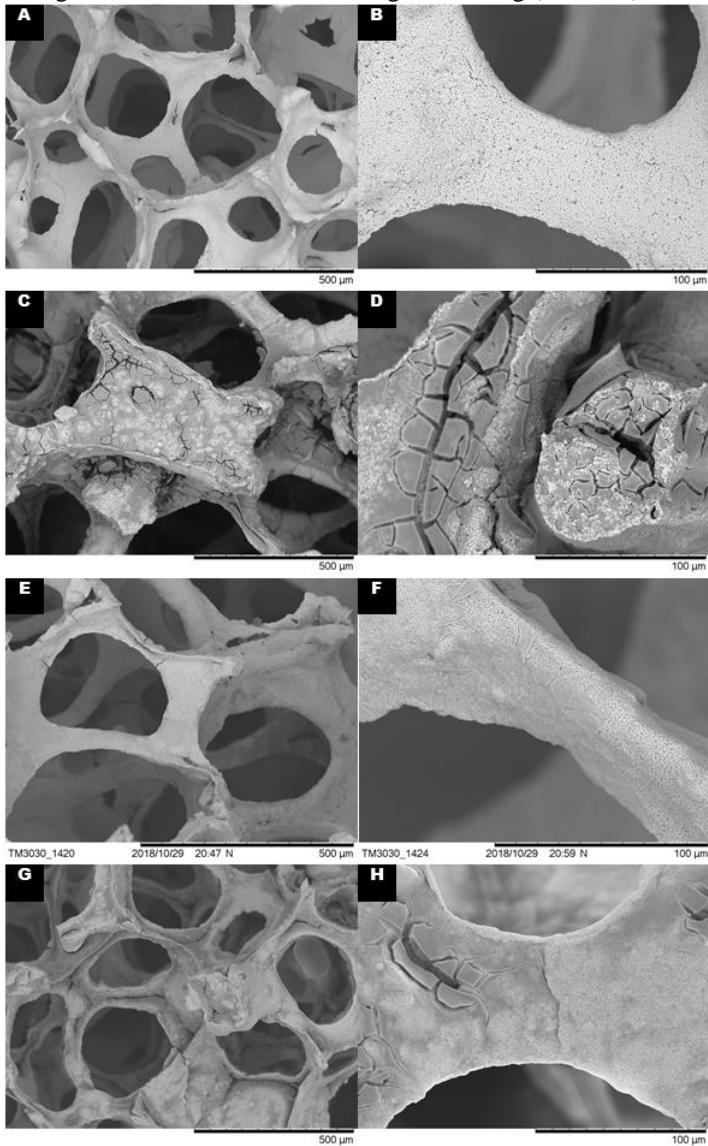
The microstructure is composed of approximately 77% of zirconia phase and 33% of the glassy phase. Also, a thin, less cracked and homogeneously distributed bioglass layer can be seen covering the struts (Figure 6B).

As mentioned above, lower sintering temperatures were tested for this group without success. Figure 7 shows the micrograph of

zirconia at 1200 °C and it is possible to see its weak and fragile structure traduced by some collapsed parts after simple handling of the structure.

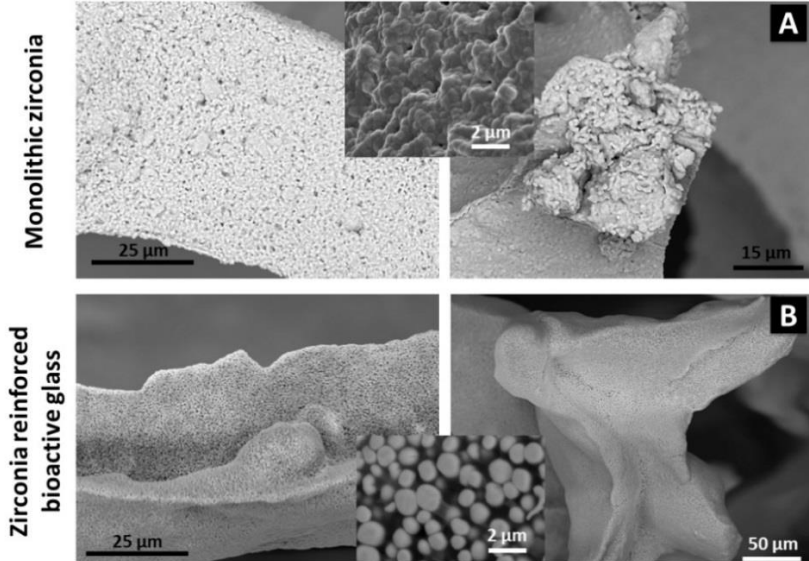
Finally, Figure 5G and H show the G4 samples, which were produced in the same way of G3 samples but received a supplementary bioactive glass coating performed at low temperature (600 °C). As depicted in Figure 5G and H, a thicker layer of BG is formed at the struts that are accompanied by some accumulation sites where cracked BG can be noticed, although in a far less extent than those seen in G2 samples.

Figure 5 - Micrographs of the different types of scaffolds produced by different routes: monolithic zirconia (A and B); zirconia with BG coating (C and D); zirconia reinforced bioactive glass (E and F); zirconia reinforced bioactive glass with additional bioactive glass coating (G and H).



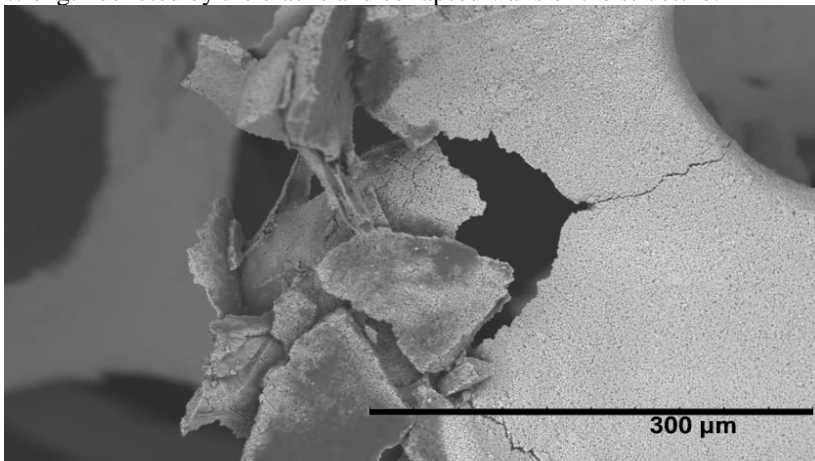
Source: Author.

Figure 6 - Detailed view on the struts of the monolithic zirconia scaffolds (A), presenting a porous microstructure, and zirconia reinforced bioactive glass scaffolds (B), where a dense microstructure and a glassy matrix with dispersed zirconia particles can be seen.



Source: Author.

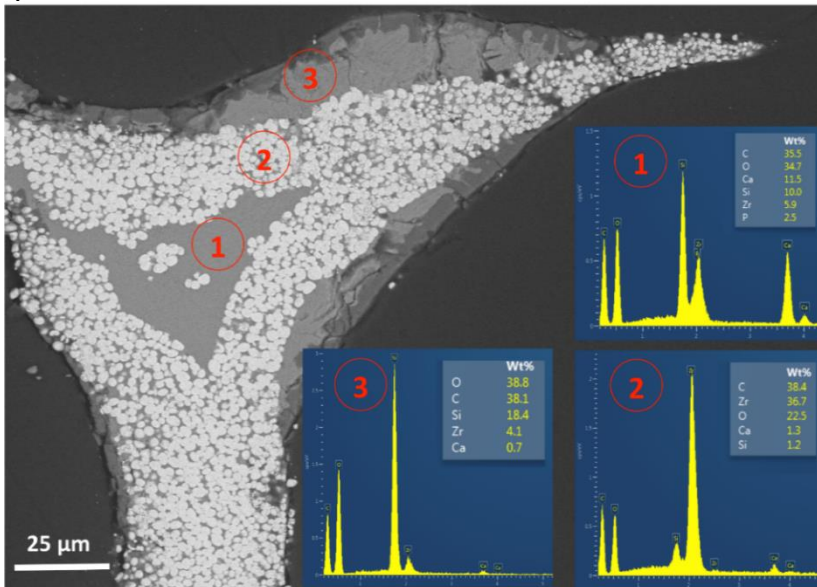
Figure 7 - Zirconia scaffold sintered at 1200 °C and exhibiting insufficient strength denoted by the cracks and collapsed walls of the structure.



Source: Author.

Figure 8 shows a detailed cross-section view of a strut from zirconia reinforced bioactive glass scaffold (G3). In this micrographs it is possible to see the complete infiltration of the bioactive glass in the zirconia template, and complete filling of the internal voids typically created by the sublimation of the polyurethane sponge used in the replica process, which can be harmful to the mechanical properties of the scaffolds (Zone 1) (HUM; BOCCACCINI, 2018). Zone 1 and 3 both present only BG58S, while zone 2 is a glassy matrix filled with zirconia particles (see EDS spectra in Figure 8). With this image, it becomes clear that the infiltration of the bioactive glass occurs in all volume of the scaffold, resulting in full densified struts with no surface or internal porosity.

Figure 8 - Cross-section view of a zirconia-reinforced bioactive glass scaffold (Group 3), showing the total infiltration of the BG58S in the zirconia pre-template. It is possible to observe that the BG fills all the void spaces inside each strut of the scaffold.



Source: Author

Density

The density calculated by the Archimedes method for groups G1, G3 and G4 are presented in Table 5.

Table 5 - Density results obtained by the Archimedes method for groups G1, G3 and G4.

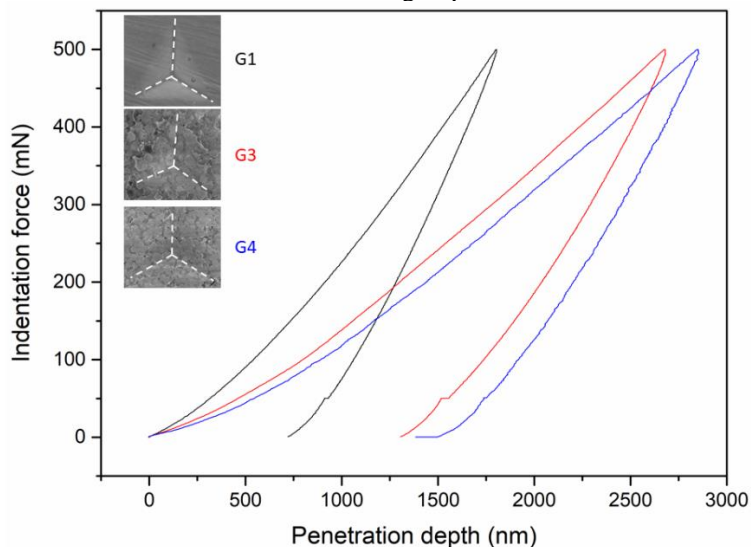
Group	Density (g/cm³)	Porosity (%)
G1	0.60 ± 0.04	90%
G3	0.63 ± 0.06	89%
G4	0.69 ± 0.09	88%

Source: Author.

Micro-indentation test

Figure 9 shows the typical depth-load hysteresis curves obtained for groups G1, G3 and G4. It can be seen that the curve of the zirconia scaffolds (G1) is different from those of the zirconia/BG scaffolds (G3 and G4), having these two specimens similar behavior. As an example, one can see that the load necessary to provoke a displacement of 1 μm in zirconia scaffolds (G1) is ~67% greater than in the zirconia/BG scaffolds (G3 and G4), thus revealing a higher stiffness for the former samples.

Figure 9 - Typical depth-load hysteresis curves obtained from micro-indentation in the struts of the different groups of scaffolds.



Source: Author.

Table 6 presents Young's modulus and Hardness values measured at the struts of the different scaffolds. The monolithic zirconia scaffolds (G1) presented the highest values (94.39 ± 12.62 GPa and 14.59 ± 0.57 GPa, respectively) while the zirconia/BG scaffolds (G3 and G4) presented lower values of Young's modulus (38.76 ± 11.20 GPa and 43.49 ± 2.16 GPa, respectively) and Hardness (4.19 ± 1.45 GPa and 4.79 ± 0.37 , respectively).

Table 6 - Hardness (GPa) and Young's modulus (GPa) of the struts of the different scaffolds.

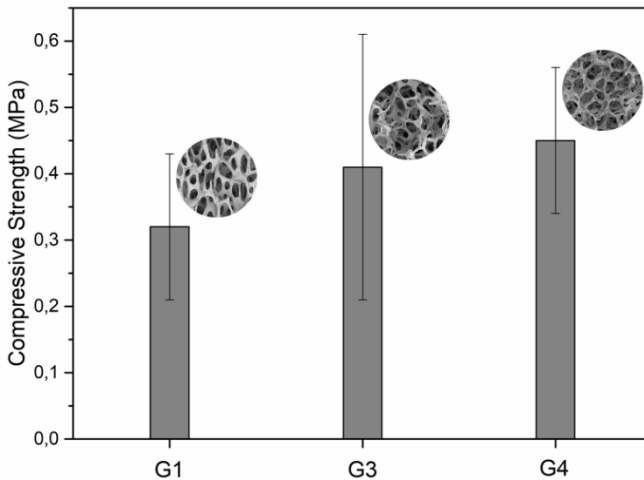
Group	Hardness (GPa)	Young's modulus (GPa)
G1	14.59 ± 0.57	94.39 ± 12.62
G3	4.19 ± 1.45	38.76 ± 11.20
G4	4.79 ± 0.37	43.49 ± 2.16

Source: Author.

Compressive strength

The compressive strength results are presented in Figure 10 and no statistical difference was found between the 3 groups ($p < 0.05$). The monolithic zirconia scaffolds of the control group (G1) exhibited a compressive strength of 0.32 ± 0.11 MPa. For the zirconia reinforced bioglass scaffolds from Group 3 (without bioglass coating) and Group 4 (with bioglass coating), slightly higher strength values were found, 0.41 ± 0.20 and 0.45 ± 0.11 MPa, respectively.

Figure 10 - Compressive strength of the monolithic zirconia scaffolds (G1); zirconia reinforced bioactive glass scaffolds: without bioglass coating (G3) and with bioactive glass coating (G4).



Source: Author.

In vitro apatite-forming assay

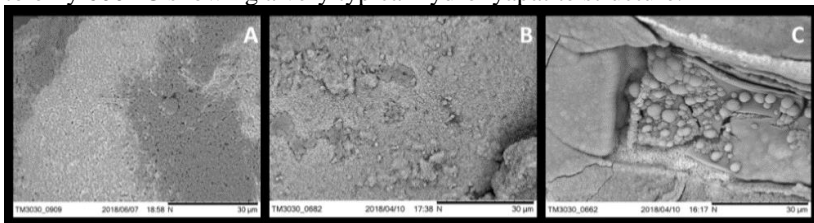
As expected, SEM images revealed that the surface from the scaffolds containing only Y-TZP continued relatively flat and did not exhibit significant changes, neither HCAp formation, after immersion in SBF for 7 days. (Figure 11A)

For the samples of G3, where BG was submitted to temperatures up to 1500 °C, SEM images showed that there was a reaction with the SBF solution, resulting in deposition of salts and calcium-phosphate based structures (Figure 11B).

For the samples of G4, that were not only infiltrated but also received a BG coating with heat treatment at 600 °C, the image shows a

very typical hydroxyapatite spherical structure, and a thick HCAp layer covering the scaffold (Figure 11C).

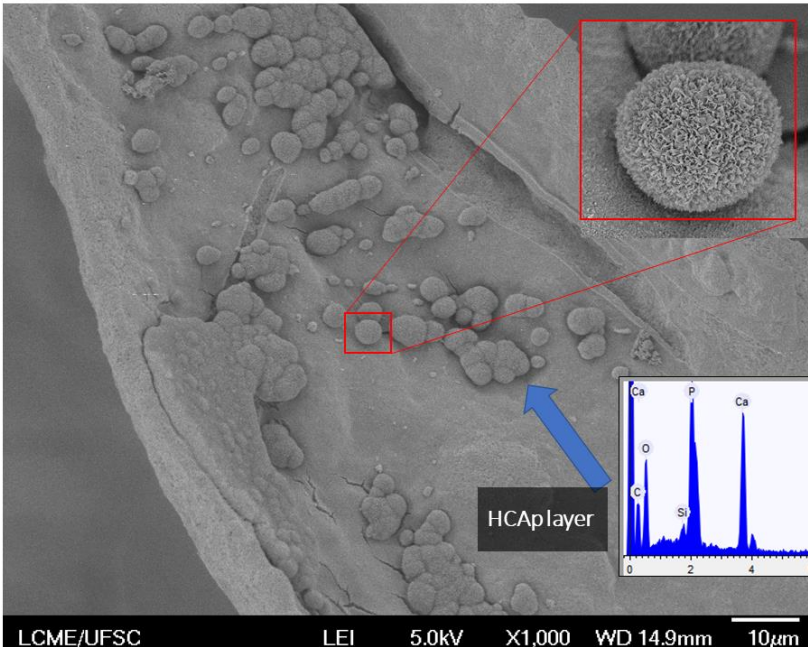
Figure 11 - Micrographs of the scaffolds after 7 days of SBF soaking: A is the G1 sample, pure zirconia scaffold and presents no significant changes; B is a sample from G3, where the BG58S was submitted to 1500 °C with no further coating, it can be observed that there was a reaction on the surface with material deposition; and C the sample from G4 with BG58S coating up to only 600 °C showing a very typical hydroxyapatite structure.



Source: Author.

A very thick hydroxyapatite layer is shown on a FEG micrograph in Figure 12. After only 7 days, almost the entire BG58S coating is covered with HCAp and it can be seen that there is the spherical typical HAp structure, which can be observed in more details from the 10000x augmentation.

Figure 12 - FEG micrograph of the hydroxyapatite layer with detailed spherical structure (10000x) on G4 scaffold after 7 days immersion in SBF. EDX analysis confirms the presence of Ca and P.



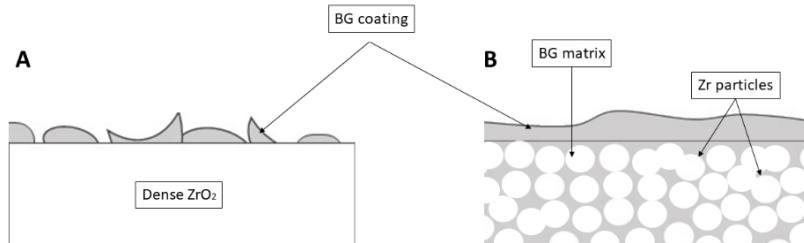
Source: Author.

3.4 DISCUSSION

The present work investigated a method for obtaining zirconia reinforced bioactive glass scaffolds for bone healing, in order to produce bioactive glass scaffolds with improved mechanical and bioactive properties. The results of the present study revealed that by infiltrating sol-gel bioactive glass (58S) into porous zirconia templates, the glass was able to fully penetrate into the porous structure, involving the zirconia particles into a glassy matrix (Figure 6) and also filling the internal void/pores left by the sublimation of the PU sponge used for the replica method (Figure 8). The morphology of the monolithic zirconia scaffolds (G1) presented rough and irregular shapes, contrasting to the smooth and organic shapes exhibited by the novel zirconia/BG scaffolds (G3 and G4) (Figure 5 and Figure 6), which better mimics the shapes of the biological materials such as the bone (FU et al., 2011).

Differences between the monolithic zirconia and zirconia/BG scaffolds were also noticed when an additional BG coating was applied (G2 and G4, respectively). The BG coated zirconia scaffolds (G2) presented an excessive cracked BG layer while a more uniform and undamaged coating was noticed on the zirconia/BG scaffolds (G4) (Figure 5 and Figure 6). The explanation for such behavior is schematically illustrated in Figure 13 and lies on the microstructure of the zirconia/BG scaffolds, which consists of a glassy matrix with dispersed zirconia particles. This microstructure makes this type of scaffolds a better substrate to receive a bioactive glass coating since there is a higher thermal (Coefficient of Thermal Expansion) and chemical (materials composition) compatibility between the coating and the substrate than in the case of the monolithic zirconia scaffold.

Figure 13 - Schematic showing the bioactive glass coating in different substrates: A) monolithic zirconia substrate (G2), where the coating has a different CTE and composition from that of the substrate and, B) the substructure consists of a BG matrix with dispersed zirconia particles, which exhibits higher compositional and thermal compatibility to the BG coating.



Source: Author.

The density of the zirconia/BG scaffolds was slightly higher than that of the monolithic zirconia (Table 5Table 5), as the residual porosity shown in the former was filled by the glass phase in the latter. The porosity (%) did not change significantly among the different groups, though, and remained ~90%.

The compressive strength of the zirconia scaffolds (G1) and the novel zirconia/BG scaffolds were not statistically different ($p > 0.05$), despite the higher mean strength values exhibited by the zirconia/BG scaffolds groups (G3 and G4), which even evidences an improvement trend over the strength of the monolithic zirconia scaffolds (G1). The results also show that the additional bioactive glass coating performed

on the G4 scaffolds did not influence the mechanical strength. So far, only one study could be found in the literature reporting the compressive strength of monolithic zirconia scaffolds.

The authors reported a compressive strength of 0.6 MPa for scaffolds with ~90% porosity, which is higher than the compressive strength found in the present study. Differences in the experimental method linked to the preparation of the ceramic suspensions and also to the sintering protocols may explain the different results. Additionally, few studies can be found in the literature on highly porous (>90% porosity) bioactive glass-scaffolds obtained from replica method (CHEN; THOMPSON; BOCCACCINI, 2006; REZWAN et al., 2006). Chen et al. reported maximum compressive strength values of ~0.35 MPa (values ranged from 0.1-0.4MPa) for 45S5 Bioglass scaffolds with ~90% porosity (CHEN; THOMPSON; BOCCACCINI, 2006). In another study, Chen et al. reported compressive strength values of 0.1-0.15 MPa for 45S5 Bioglass scaffolds with porosities of 92-94% (CHEN et al., 2008). The literature on sol-gel derived scaffolds is equally scarce (SEPULVEDA; JONES; HENCH, 2002b; XIA; CHANG, 2010), despite the known benefits of the typical hierarchical pore architecture inherent to the sol-gel process (FU et al., 2011). To date, only one study reported on the mechanical properties highly porous (~90% porosity) 58S bioactive glass scaffolds (the same as that used in the present study) obtained by the replica method. The authors reported a compressive strength of 0.16 ± 0.05 MPa for a porosity of $89.3 \pm 2.0\%$. These values highlight the challenge in producing highly porous bioactive glass scaffolds with reasonable or acceptable mechanical strength and evidence the significance of the achievements of the present study. We have here demonstrated a method of producing sol-gel derived bioactive glass scaffolds with improved mechanical properties (over 100%) over the monolithic ones, enabled by the presence of a zirconia crystalline phase (Figure 6 and Figure 8).

The Young's Modulus of the struts of the zirconia/BG scaffolds (G3 and G4) was lower than that of the monolithic zirconia (G1), 38.76 ± 11.20 , 43.49 ± 2.16 and 94.39 ± 12.62 GPa, respectively. On the other hand, the elastic modulus of sintered 45S5 BG has been reported to be in the range of (90–110 GPa) (CHEN et al., 2012; SRIVASTAVA; PYARE; SING, 2012). Considering that Young's moduli reported for cortical and cancellous bones ranges from 10-20 GPa and 0.1-5 GPa (FU et al., 2011), respectively, it can be noticed that the novel zirconia/BG scaffolds exhibit enhanced elastic compatibility to the bone relative to their counterparts.

The microstructure of the novel zirconia/BG scaffolds, where zirconia particles are spread through a glass matrix, is also expected to display improved resistance to crack propagation. This property is measured in terms of an engineering parameter called fracture toughness, denoted K_{IC} . Ceramics and glasses are very sensitive to the presence of small defects and flaws, resulting in typical K_{IC} values ranging between 0.5-1 MPa.m^{1/2}. The K_{IC} of cortical bone has been reported to range between 2-12 MPa.m^{1/2}. The fracture toughness (K_{IC}) of a glass-ceramic reinforced by zirconia particles have been shown to significantly increase with the increasing content of the zirconia phase (SANTOS et al., 2016). From the mechanical point of view, it can be said that the novel zirconia/BG scaffolds display enhanced features in terms of mechanical strength, elastic properties and damage resistance.

Although there is a criticism involving the use of an *in vitro* protocol for testing the bone bonding potential of a material and its *in vivo* relevance (BOHNER; LEMAITRE, 2009), simulated body fluid test is widely accepted and applied to evaluate the bioactivity and behavior of a material in terms of its capability to induce the formation of HCAp on its surface and hence the ability of a material to bond to bone tissue (KOKUBO; TAKADAMA, 2006; MAÇON et al., 2015). In this study, as it was expected, pure Y-TZP scaffolds did not exhibit HCAp formation after 7 days in SBF solution. The samples from G3 presented a change on its surface, indicating a reaction with the solution. Although it was not HCAp typical structures, it is possible that the bioactivity of 58S is not ultimately harmed after being exposed to temperatures up to 1500 °C since there was Ca/P based depositions. A previous study showed that its bioactivity its decreased but still present after high temperatures heat treatment (MA et al., 2010). Nevertheless, samples from G4 received an additional coating step to guarantee its ability to induce HAp formation and it was confirmed that, after 7 days of SBF immersion, a hydroxyapatite layer was formed on its surface. That confirms the bioactivity of the scaffold and the possibility of further testing.

3.5 CONCLUSIONS

This work aimed to define a processing route for the production of zirconia reinforced bioactive glass scaffolds for biomedical applications. Based on the obtained results obtained in this study, the following conclusions could be drawn:

- the production route for zirconia reinforced bioactive glass (ZRBG) scaffolds was successfully determined;
- the microstructure of ZRBG scaffolds consisted of a bioactive glass matrix with dispersed zirconia particles;
- the ZRBG scaffolds (groups G3 and G4) exhibited adequate compressive strength values (0.41 ± 0.20 and 0.45 ± 0.11 MPa, respectively), being similar to those obtained for monolithic zirconia scaffolds (group Z1) (0.32 ± 0.11 MPa);
- the ZRBG scaffolds exhibited bioactive properties, contrasting to the lack of bioactive response seen in the monolithic zirconia scaffolds. The ZRBG scaffolds with an additional BG coating (G4) showed the best results in terms of bioactive response when immersed in SBF, inducing significant HCAp formation along its surface, suggesting that further studies should be conducted with this material.

4 IN-VITRO MECHANICAL AND BIOLOGICAL EVALUATION OF ZIRCONIA REINFORCED BIOACTIVE GLASS (58S) SCAFFOLDS FOR BONE REGENERATION

4.1 INTRODUCTION

Bone is a dynamic and highly vascularized organ, capable of spontaneous self-repair through its native osteogenic potential (GALARRAGA-VINUEZA et al., 2017). Nevertheless, trauma, infection or tumours can cause critical size defects and subsequently compromise the tissue's self-healing ability. Thus, in these clinical situations, the organ repairing ability will be impaired and horizontal and vertical bone augmentation techniques will be required to repair significant bone defects (CAPLAN; BRUDER, 2001; GALARRAGA-VINUEZA et al., 2017, 2017c; LAURENCIN; KHAN; EL-AMIN, 2006; MONJE et al.).

Compared to traditional autograft and allograft applications, tissue engineering approaches, using bioactive materials such as ceramics, polymers and composites, present various advantages (SOUZA et al., 2018). Morbidity reduction, the elimination of secondary surgeries, lower risk of block graft shrinkage and reduced risk of immune rejection and pathogen transmission associated to allografts are some of the clinical benefits (LAURENCIN; KHAN; EL-AMIN, 2006; REZWAN et al., 2006; SHADJOU; HASANZADEH, 2015).

Previously, tissue replacement and fracture fixation were the main goals of a repairing surgical approach and for that, metals, including platinum, titanium, stainless steel, and some polymers were used to fabricate bone grafts. However, aiming not only to replace but also to regenerate the tissue, a new generation of materials such as bioactive ceramics have been developed and studied (JONES; HENCH, 2003; LAURENCIN; KHAN; EL-AMIN, 2006).

Among the most studied bioactive ceramics are the bioactive glasses (BGs), reported to rapidly interact with bone receptor tissues, to stimulate bone growth, promote angiogenesis, and bone repair through its ion exchange ability when in contact with body fluids (HENCH, 2015; HUPA; YLI-URPO, 2012; JONES, 2012). BGs can be defined as materials designed to obtain a specific biological response through controlled reactions of their surface (AHO et al., 2003; ORÉFICE, R. L.; PEREIRA, M. D. M.; MANSUR, 2006). Moreover, their bioactivity is linked to hydroxyl-carbonate apatite (HCAp) layer, having a structure

and composition that mimics the mineralized phase of bone (GALARRAGA-VINUEZA et al., 2018; HAMADOUCHE bone defects, showing et al., 2001). This layer is formed on the BG surface, which results in a biological and chemical match between the graft and the receptor tissue (HENCH, 2015; JONES, 2012).

BG grafts in particle format have been used to repair small and medium-sized favorable clinical results over time (HENCH, 2006; KRISHNAN; LAKSHMI, 2013; WHEELER et al., 1998). However, particles are not clinically indicated for the repair of significant defects, since they do not provide an adequate structure for vascularization, nutrition, cell proliferation, and mechanical stability (ARCOS; VALLET-REGÍ, 2010; RAMIRO-GUTIÉRREZ; WILL; BOCCACCINI, 2014). Notably, for critical horizontal and vertical defects, scaffolds are indicated since they do provide a suitable macro-structure with biological and mechanical properties that will favor and sustain bone repairing processes (HUM; BOCCACCINI, 2018; KARAGEORGIU; KAPLAN, 2005; LIU; LIM; TEOH, 2013).

A considerable disadvantage of glass derived scaffolds has been reported to be low fracture toughness and mechanical resistance (FU et al., 2011). In some cases, when these highly porous structures are obtained using the replica method with polyurethane sponges as mold, the compressive resistance can be as low as < 0.05 MPa (BOCCARDI et al., 2016). Consequently, BG scaffolds need a reinforcing component to achieve a favorable mechanical resistance that will provide satisfactory clinical outcomes when the patient is in function. In particular, zirconia is a ceramic with excellent biocompatibility, especially when in direct contact with bone (HÅVARD et al., 2004). Contrary to BGs and hydroxyapatite, zirconia is an almost bioinert material due to its *in vivo* stability (ROLDÁN et al., 2017). Furthermore, yttria stabilized zirconia possesses excellent mechanical properties such as high fracture toughness which makes this material suitable for various biomedical and dental applications. This oxide ceramic has been used in orthopedic prostheses and dental implants, since it is appropriate and resistant for high strength and fracture toughness clinical requirements (CHEVALIER, 2006; DENRY; KELLY, 2008; GOUVEIA et al., 2017; KELLY; DENRY, 2008; ÖZKURT; KAZAZOĞLU, 2011; SCHÜNEMANN et al., 2019).

Ideally, scaffolds should be bioactive, support cell adhesion and proliferation, enhance osteogenic differentiation, and provide mechanical properties to guarantee its integrity and structure stability when in contact with dynamic forces and loading (HING, 2005;

HUTMACHER, 2006; LAURENCIN; KHAN; EL-AMIN, 2006; LOH; CHOONG, 2013; MA, 2004b; MOHAMAD; BRETCANU; BOCCACCINI, 2008; REZWAN et al., 2006; TIAINEN et al., 2010). As follows, this study aimed to characterize and evaluate the *in vitro* biological response of bioactive glass scaffolds reinforced with yttria-stabilized zirconia obtained through the replica method (See Chapter 3).

4.2 MATERIALS AND METHODS

For this study, scaffolds obtained on a previous work were used, and the following materials were employed for the fabrication process (See Chapter 3):

Ceramic powder

For this study, yttria-stabilized zirconia spray-dried powder (TZ-3YSBE, TOSOH Co., Tokyo, Japan) with high purity (99% ZrO₂) and properties according to Table 7 were used. According to the supplier, the powder has a maximum particle size of 120 μm and spherical agglomerates with an average size of 60 μm.

Table 7 - Properties of commercial zirconia powder TZ-3YSB-E

Density (g/cm³)	6.05
Green density (g/cm³)	2.79
Hardness (HV10)	1250
Bending strength (MPa)	1100
Fracture toughness (MPa*m^{1/2})	5

Source: Tosoh Co.

Ceramic suspension

The zirconia suspension was prepared according to the method described elsewhere (J. Mesquita-Guimarães et al.). Suspensions thus contained 60 wt% of yttria-stabilized zirconia powder and 1 wt% of Duramax D3005, a dispersant used to adjust the pseudoplastic and thixotropic rheological behavior (J. Mesquita-Guimarães et al.).

The suspension was obtained by adding 20 ml of distilled water to 30 g of zirconia powder. It was then milled in a planetary ball mill (PM100, Retsch) for 80 min at 400 rpm for powder deagglomeration and slurry homogenization. Afterward, the dispersant Duramax was added to achieve the desired rheological behavior.

Bioactive glass 58S

The 58S bioactive glass (BG58S) (58 wt % SiO₂, 33 wt % CaO, 9 wt % P₂O₅) was synthesized by the sol-gel method. An alternative sol-gel synthesis was used when compared with others already reported (PEREIRA et al., 2014). Tetraethyl Orthosilicate (TEOS) (98%, Sigma–Aldrich, USA), triethyl phosphate (TEP) (99.8%, Sigma–Aldrich, USA) and calcium nitrate tetrahydrate (Ca(NO₃)₂·4H₂O) (Vetec, Brazil) were used as precursors of silicon, phosphorous and calcium oxide, respectively. Ethyl alcohol (EtOH, P.A., Synth, Brazil) was used as solvent of TEOS and TEP, and nitric acid (HNO₃, 68%, Vetec, Brazil) was used to dissolve Ca(NO₃)₂·4H₂O, respecting the “like dissolves like” chemical dissolution rule (BETTELHEIM et al., 2009).

First of all, to do the synthesis, the molar ratio of SiO₂, P₂O₅, and CaO were calculated respecting weight amounts of the 58S. Then, TEOS was added to EtOH in a glass beaker under magnetic stirring. The beaker was covered with paraffin film to avoid evaporation and then stirred for 10 min. TEP was added to this solution in constant agitation and stirred for 10 min. Ca(NO₃)₂·4H₂O was dissolved in 2M HNO₃ and added to water at a molar ratio TEOS: H₂O of 1:4. This mixture was added to the solution and stirred for 1 h. During solution preparation, heating was avoided to prevent solvent evaporation.

Polyurethane sponges

To serve as sacrificial templates at the replica method, polyurethane (PU) sponges of 45, 60 and 80 pores per inch (ppi) were cut into 1 cm³ cubes (10 mm x 10 mm x 10 mm).

The fabrication method of the scaffolds is described below:

Scaffolds production processes

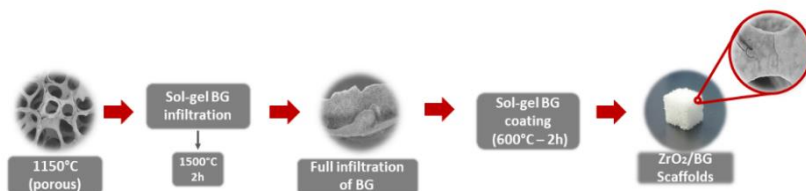
The PU sponges (45, 60 and 80 ppi) were manually impregnated with the ceramic suspension without clogging the pores and kept in a stove at 100 °C for 20 min. A pre-sintering thermal treatment at 1150 °C at 1 °C/min for 120 min was performed to eliminate the PU sponge and pre-consolidate the scaffold. The result was a pre-template of a zirconia scaffold, not fully densified but resistant enough to be manipulated.

The pre-consolidated samples went through BG58S infiltration: the samples were placed in a glass beaker containing BG58S solution inside a vacuum chamber for 10 min and then submitted to regular zirconia sintering thermal treatment (1500 °C at 5 °C/min for 120 min). This process is essential to achieve the desired microstructure, a

bioactive glass matrix with zirconia particles dispersed, as it is demonstrated in Figure 6 and with a cross-section detail on Figure 8, where it is possible to observe the BG penetration on the voids left by the PU sponge after heat treatment and consequent sublimation.

Finally, the sintered hybrid scaffolds were infiltrated in a vacuum chamber, for 10 min, and heat-treated at 600 °C for 120 min at 1 °C/min for consolidation of the bioactive glass. Since the samples were infiltrated with 58S twice (Figure 14), they are going to be named 2x 58S from now on.

Figure 14 - Flow diagram summarizing the steps involved in obtaining bioactive glass hybrid scaffolds.



Source: Author.

A previous work (See Chapter 3) showed that scaffolds which were submitted to only one 58S infiltration and heat treated at 1500 °C had a decreased bioactivity, due to the high processing temperatures. Since those samples were only analyzed through SEM images, the following study performed further tests for those samples as well and they are going to be referred to as 1x 58S.

Scaffolds with no bioactive glass, only ZrO₂, were used as a comparison group.

Mechanical characterization

Compressive strength tests were carried out in a universal mechanical testing machine (23-5S, INSTRON/EMIC, Brazil) with a 50 N load cell and 1 mm/min test rate. The tests were performed until 25% of the total height of the samples (JAIN et al., 2003; MESQUITA-GUIMARÃES et al., 2017). A total of 10 samples of each condition and porosity (45, 60 and 80 ppi) was tested.

Statistical analysis

The results were analyzed using one-way ANOVA followed by the Tukey Test. The Kolmogorov_Smirnov test was first applied to test

the assumption of normality. Differences between the compressive strength groups were tested using the t-test. P values lower than 0.05 were considered statistically significant.

In vitro apatite-forming assay

Simulated body fluid (SBF) was obtained according to Kokubo's (KOKUBO; TAKADAMA, 2006) method and its chemical composition is shown in Table 8 (GALARRAGA-VINUEZA et al., 2018; KOKUBO; TAKADAMA, 2006). For this test, samples of 60 ppi from the three conditions, including pure ZrO₂ scaffolds, to serve as a negative control group, were immersed into 30 mL of SBF solution (Ph: 7.4) in sterilized PP tubes. This test was run in triplicate. The tubes were stored in an incubator at 37 °C for periods of 12h, 24h, 72h, 1 week, 3 weeks and 4 weeks. After each period, they were removed from the solution, washed with deionized water and dried in an oven at 37 °C for 24 h. The pH change of the SBF solutions was measured after each period and sample immersion in triplicate, the mean and standard deviation (SD) was calculated accordingly.

Table 8 - Chemical composition of the SBF stock solution.

Order	Reagent	Amount
1	NaCl	8.035 g
2	NaHCO ₃	0.355 g
3	KCl	0.225 g
4	K ₂ HPO ₄ 3H ₂ O	0.231 g
5	MgCl ₂ 6H ₂ O	0.311 g
6	1.0 _M - HCl	39 mL
7	CaCl ₂	0.292 g
8	Na ₂ SO ₄	0.072 g
9	Tris	6.118 g
10	1.0 _M - HCl	0 – 5 mL

Source: (KOKUBO; TAKADAMA, 2006).

The samples` capability of forming a HCAp layer on their surface was evaluated by Scanning Electron Microscope (SEM)(TM3030 Hitachi, Japan) with Energy Dispersive X-Ray Spectroscopy (EDX), Field Emission Gun Scanning Electron Microscope (JEOL JSM-6701F (FEG), X-Ray Diffraction (XRD, D2 Phaser Bruker; at 30 kV and 10

mA utilizing CuK α radiation with the range of 2θ angles from 20 to 100, at a step size of 0.05) and Fourier Transform infrared spectroscopy (FTIR, TENSOR 27, Bruker).

In vitro cell culture tests

To evaluate the cell viability of the hybrid scaffolds 1x 58S and 2x 58S in comparison with the standard non-coated zirconia scaffolds (ZrO₂) (MESQUITA-GUIMARÃES et al., 2017) using the 60 PPI foam an osteoblast-like cell line MG-63 (Sigma-Aldrich, Germany) was used. Cells were cultured at 37 °C in an atmosphere of 95% humidified air and 5% CO₂, in an osteogenic factors solution of DMEM (Dulbecco, Germany) containing 10 vol% of fetal bovine serum (FBS, Sigma-Aldrich, Germany) and 1 vol% of penicillin/streptomycin (Life technology, Germany). Cells were grown for 48 h to confluency in 75 cm² culture flasks (Nunc, Denmark), before being harvested using Trypsin/EDTA (Sigma, Germany). They were counted by a hemocytometer (Roth, Germany) and diluted to a final concentration of 1x10⁵ cells/ml. To compare the morphology of the cells grown on the test samples, cell culture dishes were used as reference material.

Cell viability was determined by using the water-soluble tetrazolium (WST) assay. After cell cultivation, the cell culture medium was removed and samples were washed with 0.5 mL phosphate buffered saline (PBS). Afterward, 0.25 mL WST medium (containing 1 vol% of WST reagent (Cell Counting Kit-8, Sigma-Aldrich, Germany) and 99 vol% of DMEM medium) was added and incubated for 2h. After incubation, 0.1 mL of the supernatant was transferred to a 96-well culture plate and spectrometrically measured using a microplate reader (PHOMo, Anthos Mikrosysteme GmbH, Germany) at 450 nm.

For the evaluation of the attachment and distribution of the cells on the surface struts, the cell cultures were evaluated using scanning electron microscopy. The samples were prepared for the scanning electron microscope visualization. For that, the cell cultures were washed with PBS, fixed with a solution containing 3 vol% glutaraldehyde (Sigma, Germany) and 3 vol% paraformaldehyde (Sigma, Germany) in 0.2 M sodium cacodylate buffer (pH 7.4), for scanning electron microscopy analysis. All samples were dehydrated in graded ethanol series (30, 50, 70, 80, 90, 95, and 99.8 vol.%). Samples were maintained at 99.8 vol.% ethanol and critical-point dried (EM CPD300, Leica, Germany).

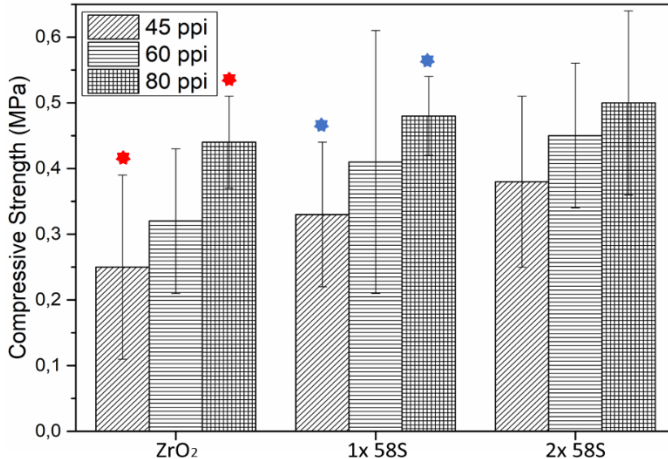
4.3 RESULTS

Mechanical characterization

The mean compressive stress results for the 45, 60 and 80 ppi scaffolds are presented on Figure 15. For the ZrO_2 scaffolds, the mean values were 0.25 ± 0.14 MPa for 45 ppi, 0.32 ± 0.11 MPa for 60 ppi and 0.44 ± 0.07 MPa for 80 ppi. For the 1x 58S samples, the mean value was 0.33 ± 0.11 , 0.41 ± 0.20 and 0.48 ± 0.6 MPa for 45, 60 and 80 ppi respectively. The samples 2x 58S presented mean values of 0.38 ± 0.13 , 0.45 ± 0.11 and 0.50 ± 0.14 MPa for 45, 60 and 80 ppi.

With statistical analysis, it can be said that there is no significant difference between the groups when each porosity is considered, which means there is no statistical difference between ZrO_2 60 ppi, 1x 58S 60 ppi and 2x 58S 60 ppi, for example. When 45, 60 and 80 ppi of the same type of scaffold are analyzed, there is a difference between 45 and 80 ppi for ZrO_2 and 1x 58 samples.

Figure 15 - Compressive strength of zirconia and bioactive glass hybrid scaffolds for 45, 60 and 80 ppi templates. The red and blue dots indicate the groups where significant statistical differences were found.



Source: Author.

In vitro apatite-forming assay

After the scaffolds immersion in SBF medium at different periods, the pH of the solutions after 12 h increased from 7.4 to 7.58 for the ZrO_2 scaffolds group, to 7.62 for 1 x 58S group, and to 7.75 for

2x 58S group (Table 9). After 4 weeks, the pH of the solution containing ZrO₂ scaffolds reached 7.74 while the solutions containing 1 x BG58S and 2 x BG58S reached a pH of 7.73 and 7.93 respectively.

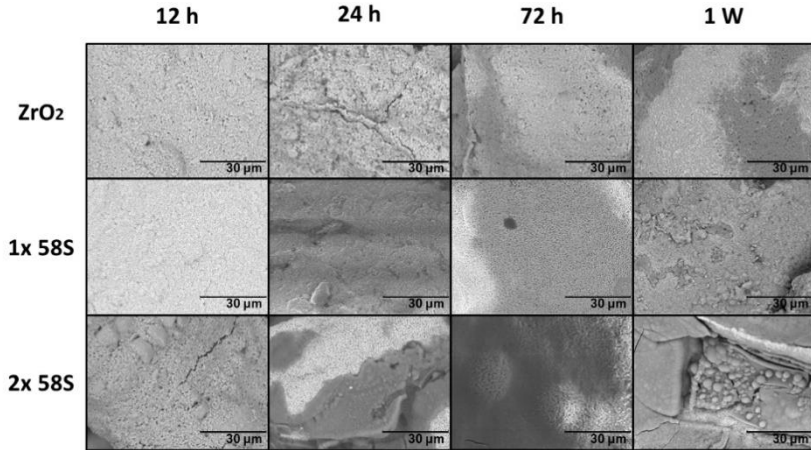
Table 9 - The pH of SBF following exposure to the scaffolds at given time points.

SBF Period	ZrO₂	1x 58S	2x 58S
12 h	7.58 ± 0.00	7.62 ± 0.00	7.75 ± 0.01
24 h	7.58 ± 0.02	7.59 ± 0.00	7.63 ± 0.02
72 h	7.68 ± 0.01	7.67 ± 0.01	7.94 ± 0.02
1 week	7.65 ± 0.01	7.66 ± 0.00	7.65 ± 0.01
4 weeks	7.74 ± 0.01	7.73 ± 0.01	7.93 ± 0.01

Source: Author.

Microscopic observations (SEM) revealed that the surface of the scaffolds containing only ZrO₂ continued relatively flat and did not exhibit significant changes, neither HCAp formation after 7 days of SBF immersion). For the hybrid scaffolds, containing 58S, the samples 1x 58S did not show significant changes on its surface until 7 days of SBF soaking. After this period, it was possible to observe calcium-phosphates depositions along its surface, although HCAp typical structures could not be identified on the scaffold (Figure 16). On the other hand, while for 12 hours of SBF immersion no considerable changes on 2 x 58S sample surface could be observed, the micrographs after 24h of SBF immersion showed a typical hydroxyapatite spherical structure on its surface. After 7 days of SBF immersion, 2 x 58S samples micrographs revealed a thick HCAp layer covering the scaffold structure.

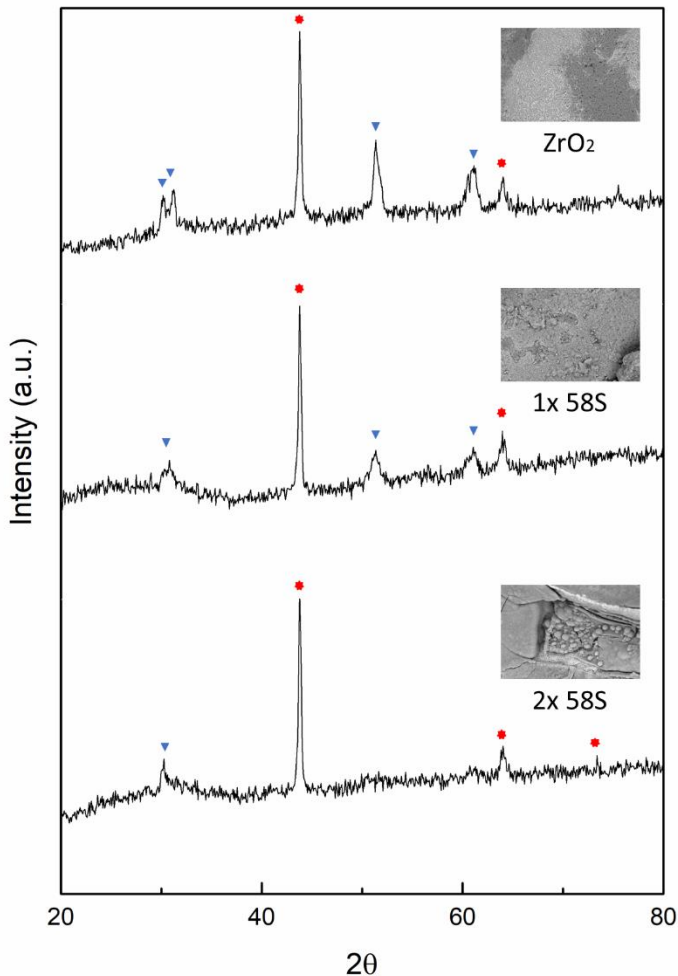
Figure 16 - Micrographs of the scaffolds after 12 h, 24 h, 72 h and 7 days of SBF soaking: Pure yttria-stabilized zirconia scaffolds do not present significant changes on its surface. After 7 days there are calcium-phosphate depositions on 1x 58S surface. The hybrid scaffolds 2x 58S present typical HCAp structures from 24 h of SBF with a thick HCAp layer after 7 days.



Source: Author.

The XRD patterns of the three samples are shown in Figure 17. All samples reveal the tetragonal zirconia characteristic peak at 30.2° and a high-intensity diffraction peak at 43.8° , which is assigned to (113) hydroxyapatite crystal plane (JCPDS no. 09-0432). All samples also present a (304) hydroxyapatite crystal plane at 64° and the sample 2x58S shows an additional hydroxyapatite peak at around 73.5° .

Figure 17 - XRD patterns of samples after SBF immersion for 7 days. The red dots indicate characteristic peaks for HCAp crystal planes according to (JCPDS no. 09-0432). The blue triangles represent peaks for ZrO_2 according to (JCPDS no. 14-0534) and 9486.



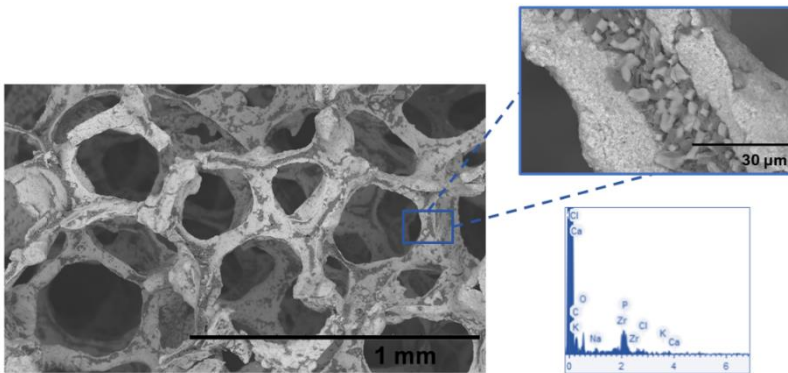
Source: Author.

The microscopic observations could be correlated with the chemical analyses of the samples. EDX analysis revealed that after 4 weeks of SBF soaking, 1x 58S samples presented calcium-phosphates depositions along its surface, as can be seen in Figure 18. EDX analysis

confirmed the presence of Ca and P in this sample. Also, after 4 weeks of SBF immersion, the entire 2x 58S scaffold showed the presence of a thick HCAp layer which was confirmed by EDX analysis exhibiting Ca and P content as shown in Figure 19.

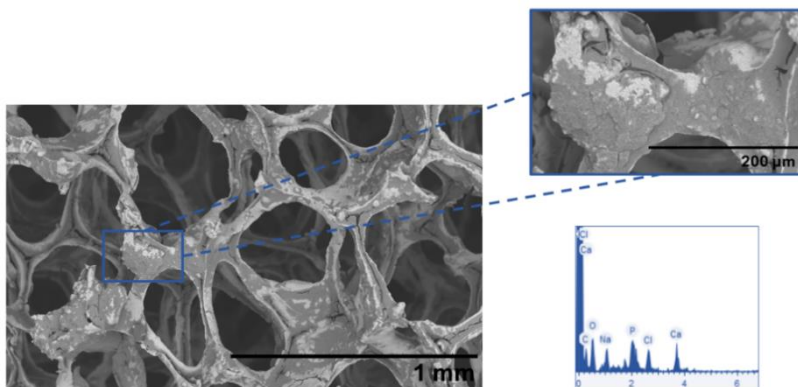
Conversely, for the sample containing only ZrO₂, the depositions along the scaffold surface were mostly salts and indeed not HCAp structures after 4 weeks of SBF immersion. This is shown by the EDX analysis where no Ca and P were present as expected (Figure 20).

Figure 18 - SEM image and EDX analysis of a 1x 58S scaffold after 4 weeks of SBF soaking. It is possible to observe Ca-P depositions along its surface.



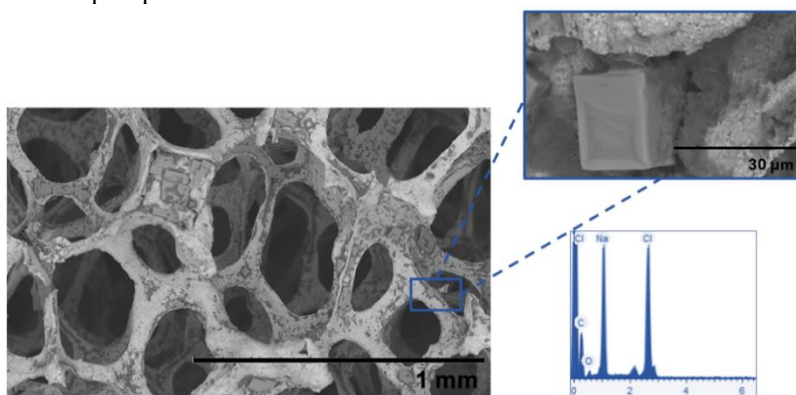
Source: Author.

Figure 19 - SEM micrograph of a hybrid scaffold (2x 58S scaffold) after 4 weeks of SBF immersion. A thick HCAp layer is covering almost the entire surface of the sample.



Source: Author.

Figure 20 - ZrO₂ scaffold after 4 weeks of SBF immersion. For the EDX analysis, it can be concluded that these depositions are salt crystals and not calcium-phosphate structures.

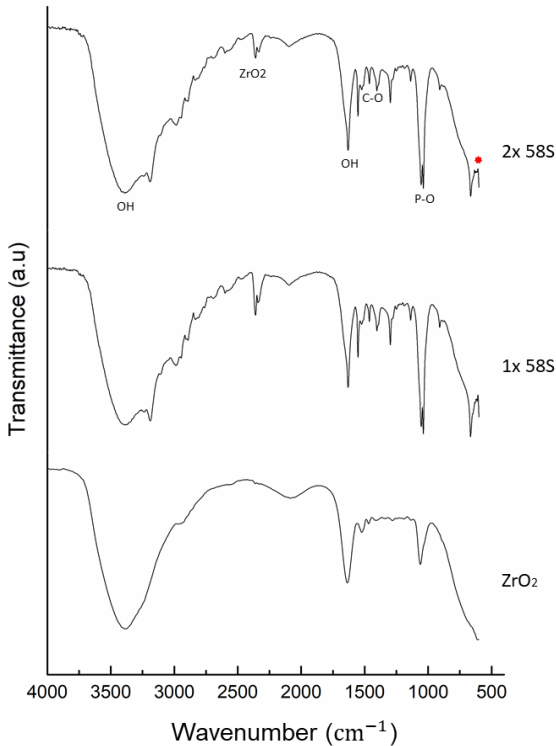


Source: Author.

Furthermore, to confirm the atomic structure of the deposited minerals, FTIR analyses were performed and shown in Figure 21. The FTIR spectra of all samples containing 58S presented the characteristic peaks attributed to HCAp layer formation as a doublet at around 600 cm^{-1} , corresponding to the bending mode of crystalline phosphate P-O and P-O stretching mode at $\sim 1050\text{ cm}^{-1}$. On the other hand, the

spectrum of ZrO_2 scaffolds after 4 weeks of SBF immersion indicated the absence of the mentioned double peak. Besides the bands above mentioned, carbonate adsorption bands around 1400 cm^{-1} were also detected for the samples containing 58S.

Figure 21 - FTIR spectra of samples after 4 weeks of soaking in SBF. The red spot identifies the double peak characteristic of HCAp formation.

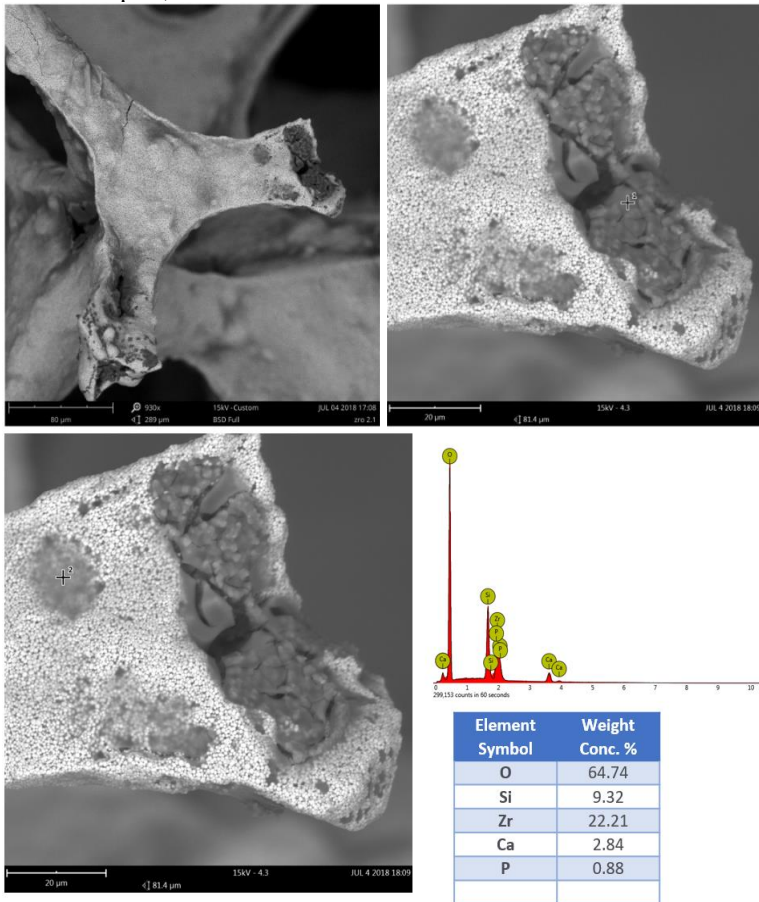


Source: Author.

In vitro cell culture tests

The samples were inspected via SEM and also the Ca/P ratio was determined by using EDS, previous to cell culture, as illustrated in Figure 22.

Figure 22 - SEM micrographs and EDS analysis of the Ca/P ratio on the 2x58S samples, before cell culture.



Source: Author.

In SEM micrographs is possible to observe the presence of a thin 58S coating and the fill-in of the foam struts with 58S. The EDS analysis indicates a Ca/P ratio value of 3.3, which is very close to the original 3.6.

First, as a control for the potentialities of a succeeded cell culture, samples were placed in DMEM+FCS+PENSTREP solution and incubated during 48h and 96h, after which the pH was measured. Table

10 exhibits the pH values of all sample groups after 48 and 96 hours of incubation in DMEM + FCS + PENSTREP solution.

Table 10 - pH values of the samples immersed on DMEM solution after 48 and 96 hours of incubation.

	DMEM (REF)	ZrO₂	1x 58S	2x 58S
48h (2 days)	7.91 ± 0.03	7.92 ± 0.02	7.90 ± 0.00	7.92 ± 0.02
96h (4 days)	7.90 ± 0.01	7.84 ± 0.0	7.84 ± 0.00	7.86 ± 0.01

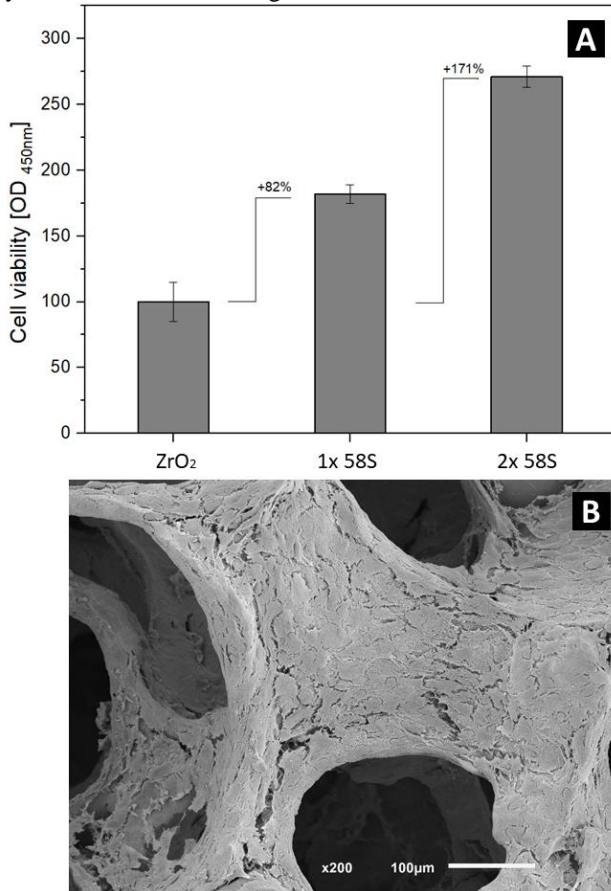
Source: Author.

The pH values vary in the range of 7.84 – 7.92, which will not cause any toxic effect on cells. It was considered that the reference value of DMEM+FCS+PENSTREP was in the acceptable range. Therefore, no additional correction of the pH was required.

In Figure 23A, cell viability results of MG-63 osteoblast-like cells on the uncoated and hybrid scaffolds 60 ppi open cell structures after 7 days of cultivation in an osteogenic medium is shown.

Figure 23B shows the MG-63 osteoblast-like cells on the 2x 58S sample attached and showing a high coverage of cells on the surface struts.

Figure 23 - a) Cell viability (by WST) results of MG-63 osteoblast-like cells on the uncoated and hybrid scaffolds after 7 days of cultivation. b) SEM image of the MG-63 osteoblast-like cells on the hybrid scaffolds 2x 58S after 7 days of cultivation in osteogenic medium.



Source: Author.

4.4 DISCUSSIONS

The present work characterized the mechanical behavior and bioactivity of BG scaffolds reinforced with yttria-stabilized zirconia for bone repair and augmentation applications, developed on previous work (See Chapter 3). The presented results support the previous study, where it was demonstrated the 60 ppi hybrid scaffolds did not present affected

mechanical resistance when compared to zirconia scaffolds and the samples infiltrated and coated with 58S (2x 58S) presented bioactivity correlated to HCAP formation after SBF soaking. It also showed that the samples where 58S went through temperatures high as 1500 °C (1x 58S) still presented some bioactivity, as indicated by FTIR and EDX analyses.

The compressive strength of the zirconia scaffolds and the novel zirconia/BG scaffolds were not statistically different ($p>0.05$), despite the higher mean strength values exhibited by the zirconia/BG scaffolds (1x 58S and 2x 58S), which even evidences an improvement trend over the strength of the monolithic zirconia scaffolds. The results also show that the additional bioactive glass coating performed on the 2x 58S scaffolds did not influence the mechanical strength. When the porosity is compared for each group of scaffolds separately, the only group that does not present a significant difference is 2x 58S. For ZrO_2 and 1x 58S, there is a statistical difference between 45 and 80 ppi. Which means not only the number and size of pores must be considered, but also the need for mechanical resistance when choosing a scaffold for an application.

The literature regarding compressive strength of both monolithic zirconia scaffolds and bioactive glass scaffolds is scarce. The authors of the only study that could be found reported a compressive strength of 0.6 MPa for zirconia scaffolds with ~90% porosity. Although it is higher than the results found in the present work, it may be explained by differences in the experimental method, such as preparation of the ceramic suspension and heat treatments. Additionally, Chen et al. reported values ranging from 0.1-0.4 MPa for 45S5 Bioglass scaffolds with ~90% porosity (CHEN; THOMPSON; BOCCACCINI, 2006b) and 0.1-0.15 MPa for 45S5 Bioglass scaffolds with porosities of 92-94% (CHEN et al., 2008). To date, only one study reported on the mechanical properties highly porous (~90% porosity) 58S bioactive glass scaffolds (the same as that used in the present study) obtained by the replica method. The authors reported a compressive strength of 0.16 ± 0.05 MPa for a porosity of $89.3\pm 2.0\%$. These values highlight the challenge in producing highly porous bioactive glass scaffolds with reasonable or acceptable mechanical strength and evidence the significance of the achievements of the present study.

Although there is criticism involving the use of an *in vitro* protocol for testing the bone bonding potential of a biomaterial and its *in vivo* relevance (BOHNER; LEMAITRE, 2009), simulated body fluid test is widely accepted and applied to evaluate the bioactivity and behavior of a material in terms of its capability to induce the formation

of HCAp on its surface and so the ability of a material to bond to bone tissue (GALARRAGA-VINUEZA et al., 2018; KOKUBO; TAKADAMA, 2006; MAÇON et al., 2015). In the present study, as it was expected, 58S infiltrations improved the scaffolds bioactivity. Pure ZrO_2 scaffolds did not exhibit significant HCAp formation even after 4 weeks in SBF immersion. X. Liu et al. (LIU et al., 2006) demonstrated that zirconia could show apatite precipitation after a period of SBF immersion and, although the SEM images do not show significant changes on its surface, XRD and FTIR indicate there is some bioactivity since there are peaks for HCAp formation on the samples. J. Ma et al. (MA et al., 2010) demonstrated on a previous work that the bioactivity of 58S is harmed but not wholly lost when exposed to temperatures as high as 1200 °C, due to its crystallization. The present study showed that when 58S was exposed to 1500 °C (1x 58S), the same behavior was observed. It took longer for HCAp deposition and was not possible to microscopically observe the typical HCAp spherical structure on the surface of scaffolds containing 1x 58S, but XRD and FTIR present the peaks for the hydroxyapatite formation. However, the 2 x 58S scaffolds did exhibit visible HCAp formation after only 24h of SBF soaking. Subsequently, a solid layer on its surface became thicker and covered almost the entire scaffold after 4 weeks of immersion. This was correlated with the XRD, EDX and FTIR results

Nevertheless, FTIR analysis of both scaffolds containing 58S BG presented the same peaks for HCAp presence after 4 weeks of SBF soaking. As follows, BG 58S containing samples did have HCAp formation and were bioactive after 1 month of immersion. Still, 2x 58S BG scaffolds showed more favorable results, since within only 24 hours it was already bioactive meaning that only one day after grafting the scaffold will start inducing a favorable biological response at the receptor tissues (COLEMAN, 2009; GALARRAGA-VINUEZA et al., 2018).

Additionally, the pH of the SBF solution increased mainly for the scaffold containing 2 x 58S after 4 weeks of immersion. The pH increased from 7.4 to 7.9, presenting a more alkaline medium. As known, an alkaline medium prevents bacteria proliferation, showing the antibacterial property of BGs (GALARRAGA-VINUEZA et al., 2017a, 2018). These results are supported by previous studies, Gholami et al. (GHOLAMI et al., 2017) showed that during immersion 58S BG, the pH of the solution increased from 7.4 to 7.9 in 24h, due to the exchange of cations from the glass with H^+ from the medium. According to Arnett

(ARNETT, 2003), a small extent of alkalosis is likely to present a bone-sparing effect, helping to prevent osteoporosis due to calcium losses, while acidosis can cause undesirable bone loss over time.

The *in vitro* cell culture tests performed in an osteogenic medium exhibited constant pH values and inside the expected ranges. Czekanska et al. (CZEKANSKA et al., 2012) explained that for osteoblastic cells a variety of basic medium types are available, like DMEM, and the concentration of additives, can vary depending on the type of medium and its pH. On the other hand, the cell viability results present an increase of more than 80% for the condition of each sample. Cell viability is considered to be right when existing an increment between 80 to 90 %. Therefore, the results show an increase of cell viability with the increase of the 58S coating content. The SEM image reveals a high coverage of cells. The cells are well spread along the struts presenting a uniform layer of cells-cells contacts. These results are correlated with the SBF mentioned outcomes which show a higher HCAp formation on samples containing 2 x 58S BG content. As follows, the HCAp layer may enhance the osteoblast adhesion over the scaffold surface.

4.5 CONCLUSIONS

This work aimed to characterize and evaluate the mechanical and the *in vitro* biological response of bioactive glass scaffolds reinforced with yttria-stabilized zirconia obtained through the replica method for biomedical applications. Based on the obtained results obtained in this study, the following conclusions could be drawn:

- The presence of 58S does not affect the mechanical resistance of the scaffolds and with ZrO₂ as reinforcement, the values are the same as ZrO₂ pure scaffolds for this replica method;
- As expected, zirconia did not exhibit apparent bioactive properties, since no significant HCAp formation has been observed after 4 weeks of SBF immersion. On the other hand, the samples containing bioactive glass 58S were able to produce HCAp;
- Despite the high processing temperatures, 1x 58S samples were still able to present a less pronounced bioactive response, while that found in the 2x 58S was extensively higher;
- The 2x 58S samples rapidly induced HCAp deposition, evidenced by the extensive formation after the first 24 hours of SBF;

- The pH of the osteogenic medium was not affected during 96 h (4 days) of test;
- The zirconia/BG samples presented enhanced cell viability (over 80%) in osteogenic medium relative to pure zirconia scaffolds;
- The zirconia/BG scaffolds presented a full coverage of cells well spread along the struts presenting cells-cells contacts.

5 GENERAL CONCLUSIONS AND SUGGESTIONS

5.1 CONCLUSIONS

The study aimed to obtain BG 58S/ZrO₂ scaffolds with satisfactory bioactivity provided by the bioactive glass and improved mechanical resistance due to the presence of zirconia. The following conclusions could be drawn:

- When an intermediate BG58S infiltration is performed before the sintering heat treatment, the bioactive glass penetrates the porous zirconia struts creating a glassy matrix and filling the void left by PU sponges sublimation;
- The presence of BG58S does not harm the mechanical resistance of the zirconia scaffolds, i.e. the zirconia/BG scaffolds exhibited a compressive strength similar to that of pure zirconia and significantly higher than those of pure BG;
- The zirconia/BG scaffolds comprising a BG58S coating exhibited the best bioactive response, indicated by the extensive HCAp formation when immersed in SBF medium;
- The elevated temperature heat treatment harms the bioactivity of BG58S but it does not completely destroy it, there was evidence of HCAp formation on the surface of the scaffolds;
- The zirconia/BG scaffolds presented good cell viability in osteogenic medium and full coverage of cells well spread along the struts.

5.2 SUGGESTIONS

After this work, some points indicate the need for improvement, suggesting that future works can be carried out:

- An investigation of how to improve mechanical resistance of the scaffolds without changing its geometry;
- A study to determine more precisely how bioactive are the scaffolds after BG58S is submitted to high temperatures such as 1500 °C;
- Reproduce the same processes using a different ceramic phase and characterize its properties;

REFERENCES

- AHO, A. J.; SUOMINEN, E.; ALANEN, A.; YLI-URPO, A.; KNUUTI, J.; AHO, H. J. Remodeling of the tibia after grafting of a large cavity with particulate bioactive glass-hydroxylapatite - Case report on treatment of fibrous dysplasia with 13 years' follow-up. **Acta Orthopaedica Scandinavica**, Department of Surgery, Turku University Hospital, POB 52, FI-20520 Turku, Finland, v. 74, n. 6, p. 766–770, 2003.
- ARCOS, D.; VALLET-REGÍ, M. Sol-gel silica-based biomaterials and bone tissue regeneration. **Acta Biomaterialia**, Departamento de Química Inorganica y Bioinorganica Ftad. Farmacia, Universidad Complutense de Madrid, Networking Research Center on Bioengineering, Biomaterials and Nanomedicine, CIBER-BBN, Madrid, Spain, v. 6, n. 8, p. 2874–2888, 2010.
- ARNETT, T. Regulation of bone cell function by acid–base balance. **Proceedings of the Nutrition Society**, [s. l.], v. 62, n. 02, p. 511–520, 2003.
- BATH, S. V. **Biomaterials**. Nova Dheli: Narosa Publishing House, 2002.
- BELLUCCI, D.; CANNILLO, V.; SOLA, A. A new highly bioactive composite for bone tissue repair. **International Journal of Applied Ceramic Technology**, [s. l.], v. 9, n. 3, p. 455–467, 2012.
- BETTELHEIM, F.; BROWN, W.; CAMPBELL, M.; FARRELL, S.; TORRES, O. **Introduction to General, Organic, and Biochemistry**. 10. ed. [s.l.] : Cengage Learning, 2009.
- BIRRER, N. . Materiais cerâmicos do sistema mullita zirconia e zircão; propriedades mecânicas, de fratura e comportamento frente ao choque térmico. [s. l.], p. 297, 2009.
- BOCCARDI, E.; PHILIPPART, A.; MELLI, V.; ALTOMARE, L.; DE NARDO, L.; NOVAJRA, G.; VITALE-BROVARONE, C.; FEY, T.; BOCCACCINI, A. R. Bioactivity and Mechanical Stability of 45S5 Bioactive Glass Scaffolds Based on Natural Marine Sponges. **Annals of Biomedical Engineering**, [s. l.], v. 44, n. 6, p. 1881–1893, 2016.

BOHNER, M.; LEMAITRE, J. Can bioactivity be tested in vitro with SBF solution? **Biomaterials**, [s. l.], v. 30, n. 12, p. 2175–2179, 2009. Disponível em: <<http://dx.doi.org/10.1016/j.biomaterials.2009.01.008>>

BURR, D. B.; ALLEN, M. R. **Basic and Applied Bone Biology**. [s.l.] : Elsevier, 2014.

CAPLAN, A. I.; BRUDER, S. P. Mesenchymal stem cells: Building blocks for molecular medicine in the 21st century. **Trends in Molecular Medicine**, [s. l.], v. 7, n. 6, p. 259–264, 2001.

CHEN, Q. Z.; EFTHYMIU, A.; SALIH, V.; BOCCACCINI, A. R. Bioglass®-derived glass-ceramic scaffolds: Study of cell proliferation and scaffold degradation in vitro. **Journal of Biomedical Materials Research - Part A**, [s. l.], 2008.

CHEN, Q. Z.; THOMPSON, I. D.; BOCCACCINI, A. R. 45S5 Bioglass®-derived glass-ceramic scaffolds for bone tissue engineering. **Biomaterials**, [s. l.], 2006.

CHEN, Q. Z.; XU, J. L.; YU, L. G.; FANG, X. Y.; KHOR, K. A. Spark plasma sintering of sol-gel derived 45S5 Bioglass®-ceramics: Mechanical properties and biocompatibility evaluation. **Materials Science and Engineering C**, [s. l.], 2012.

CHEVALIER, J. What future for zirconia as a biomaterial? **Biomaterials**, [s. l.], v. 27, n. 4, p. 535–543, 2006.

COLEMAN, N. J. Aspects of the in vitro bioactivity and antimicrobial properties of Ag⁺- and Zn²⁺-exchanged 11 A... tobermorites. **Journal of Materials Science-Materials in Medicine**, Univ Greenwich, Sch Sci, Chatham ME4 4TB, Kent, England. Coleman, NJ (reprint author), Univ Greenwich, Sch Sci, Chatham ME4 4TB, Kent, England. nj_coleman@yahoo.co.uk, v. 20, n. 6, p. 1347–1355, 2009.

CZEKANSKA, E. M.; STODDART, M. J.; RICHARDS, R. G.; HAYES, J. S. In search of an osteoblast cell model for in vitro research. **European Cells and Materials**, [s. l.], v. 24, p. 1–17, 2012.

DENRY, I.; KELLY, J. R. State of the art of zirconia for dental applications. **Dental Materials**, [s. l.], v. 24, n. 3, p. 299–307, 2008.

DEVILLE, S.; GUÉNIN, G.; CHEVALIER, J. Martensitic transformation in zirconia Part I. Nanometer scale prediction and measurement of transformation induced relief. **Acta Materialia**, [s. l.], v. 52, n. 19, p. 5697–5707, 2004.

DO VALE PEREIRA, R. **Arcabouço compósito biodegradável produzido via sinterização seletiva a laser com matriz de Policaprolactona e partículas dispersas de Biovidro 58S**. 2011. Universidade Federal de Santa Catarina, [s. l.], 2011.

DOS SANTOS, C.; ELIAS, C. N. Comparação das propriedades e biocompatibilidade de blocos de zircônia nacionais e importados para uso em prótese dentárias. [s. l.], [s.d.].

FABRIS, S.; PAXTON, A. T.; FINNIS, M. W. A stabilization mechanism of zirconia based on oxygen vacancies only. **Acta Materialia**, [s. l.], v. 50, n. 20, p. 5171–5178, 2002.

FU, Q.; SAIZ, E.; RAHAMAN, M. N.; TOMSIA, A. P. Bioactive glass scaffolds for bone tissue engineering: State of the art and future perspectives. **Materials Science and Engineering C**, [s. l.], v. 31, n. 7, p. 1245–1256, 2011. Disponível em: <<http://dx.doi.org/10.1016/j.msec.2011.04.022>>

GALARRAGA-VINUEZA, M. E.; MESQUITA-GUIMARÃES, J.; MAGINI, R. S.; SOUZA, J. C. M.; FREDEL, M. C.; BOCCACCINI, A. R. Anti-biofilm properties of bioactive glasses embedding organic active compounds. **Journal of Biomedical Materials Research Part A**, [s. l.], v. 105, n. 2, p. 672–679, 2017. a.

GALARRAGA-VINUEZA, M. E.; MEZQUITA-GUIMARAES, J.; FREDEL, M.; MAGINI, R.; SOUZA, J.; BOCCACCINI, A. R. Mesoporous bioactive glass embedding propolis and cranberry antibiofilm compounds. **Journal of Biomedical Materials Research - Part A**, [s. l.], 2018.

GALARRAGA-VINUEZA, M. E.; PASSONI, B.; BENFATTI, C. A. M.; MESQUITA-GUIMARÃES, J.; HENRIQUES, B.; MAGINI, R. S.; FREDEL, M. C.; MEERBEEK, B. V.; TEUGHEL, W.; SOUZA, J. C. M. Inhibition of multi-species oral biofilm by bromide doped bioactive glass. **Journal of Biomedical Materials Research - Part A**, [s. l.], v.

105, n. 7, 2017. b.

GALARRAGA-VINUEZA, M. E.; PASSONI, B.; BENFATTI, C. A. M.; MESQUITA-GUIMARÃES, J.; HENRIQUES, B.; MAGINI, R. S.; FREDEL, M. C.; MEERBEEK, B. V.; TEUGHEL, W.; SOUZA, J. C. M. Inhibition of multi-species oral biofilm by bromide doped bioactive glass. **Journal of Biomedical Materials Research Part A**, [s. l.], 2017. c.

GHOLAMI, S.; LABBAF, S.; HOUREH, A. B.; TING, H. K.; JONES, J. R.; NASR ESFAHANI, M. H. Long term effects of bioactive glass particulates on dental pulp stem cells in vitro. **Biomedical Glasses**, [s. l.], v. 3, n. 1, p. 96–103, 2017.

GOMEZ-VEGA, J. M.; SAIZ, E.; TOMSIA, A. P.; OKU, T.; SUGANUMA, K.; MARSHALL, G. W.; MARSHALL, S. J. Novel bioactive functionally graded coatings on Ti6Al4V. **Advanced Materials**, [s. l.], v. 12, n. 12, p. 894–898, 2000.

GOUVEIA, P. F. **Caracterização de resíduos de zircônia de uso odontológico resultantes do processo de fabricação CAD/CAM**. 2016. Universidade Federal de Santa Catarina, [s. l.], 2016.

GOUVEIA, P. F.; SCHABBACH, L. M.; SOUZA, J. C. M.; HENRIQUES, B.; LABRINCHA, J. A.; SILVA, F. S.; FREDEL, M. C.; MESQUITA-GUIMARÃES, J. New perspectives for recycling dental zirconia waste resulting from CAD/CAM manufacturing process. **Journal of Cleaner Production**, [s. l.], v. 152, p. 454–463, 2017.

HAMADOUCHE, M.; MEUNIER, A.; GREENSPAN, D. C.; BLANCHAT, C.; ZHONG, J. P.; LA TORRE, G. P.; SEDEL, L. Long-term in vivo bioactivity and degradability of bulk sol-gel bioactive glasses. **Journal of biomedical materials research**, [s. l.], v. 54, n. 4, p. 560–6, 2001.

HÁVARD, H.; WILL, J.; KÖHLER, A.; HOPFNER, U.; AIGNER, J.; WINTERMANTEL, E. Ceramic TiO₂-foams: characterisation of a potential scaffold. **Journal of the European Ceramic Society**, [s. l.], 2004.

HENCH, L. L. Bioceramics: from concept to clinics. **American**

Ceramic Society, [s. l.], 1991.

HENCH, L. L. The story of Bioglass®. **Journal of Materials Science: Materials in Medicine**, Department of Materials, Tissue Engineering and Regenerative Medicine Centre, Imperial College London, Prince Consort Road, London, SW7 2AZ, United Kingdom, v. 17, n. 11, p. 967–978, 2006.

HENCH, L. L. Opening paper 2015- Some comments on Bioglass: Four Eras of Discovery and Development. **Biomedical glasses**, [s. l.], v. 1, n. 1, p. 1–11, 2015. Disponível em: <<https://www.degruyter.com/view/j/bglass.2015.1.issue-1/bglass-2015-0001/bglass-2015-0001.xml>>

HING, K. Bioceramic bone graft substitutes: Influence of porosity and chemistry. **Int J Appl Ceram Technol**, [s. l.], 2005.

HOLZSWARTH, J. M.; MA, P. X. Biomimetic Nanofibrous Scaffolds for Bone Tissue Engineering. **Biomaterials**, [s. l.], v. 32, n. 36, p. 9622–9629, 2012.

HOPPE, A.; GÜLDAL, N. S.; BOCCACCINI, A. R. A review of the biological response to ionic dissolution products from bioactive glasses and glass-ceramics. **Biomaterials**, [s. l.], v. 32, p. 2757–2774, 2011.

HUM, J.; BOCCACCINI, A. R. Collagen as Coating Material for 45S5 Bioactive Glass-Based Scaffolds for Bone Tissue Engineering. [s. l.], 2018.

HUPA, L.; YLI-URPO, A. Dental Applications of Glasses. In: **Bio-Glasses: An Introduction**. Process Chemistry Centre, Åbo Akademi University, Biskopsgatan, Åbo, Finland: John Wiley and Sons, 2012. p. 159–175.

HUTMACHER, D. Scaffolds in tissue engineering bone and cartilage. **Biomaterials**, [s. l.], 2000.

HUTMACHER, D. W. Scaffolds in tissue engineering bone and cartilage. **The Biomaterials: Silver Jubilee Compendium**, [s. l.], v. 21, p. 175–189, 2006.

JAIN, V.; JOHNSON, R.; GANESH, I.; SAHA, B. P.; MAHAJAN, Y. R. Effect of rubber encapsulation on the comparative mechanical behaviour of ceramic honeycomb and foam. **Materials Science and Engineering A**, [s. l.], v. 347, n. 1–2, p. 109–122, 2003.

JONES, J. R. Review of bioactive glass: From Hench to hybrids. **Acta Biomaterialia**, [s. l.], 2012.

JONES, J. R. Reprint of: Review of bioactive glass: From Hench to hybrids. **Acta Biomaterialia**, [s. l.], v. 23, n. S, p. S53–S82, 2015. Disponível em: <<http://dx.doi.org/10.1016/j.actbio.2012.08.023>>

JONES, J. R.; HENCH, L. L. Regeneration of trabecular bone using porous ceramics. **Current Opinion in Solid State and Materials Science**, [s. l.], v. 7, n. 4–5, p. 301–307, 2003.

JUNQUEIRA, L. C.; CARNEIRO, J. **Histologia Básica**. 12. ed. Rio de Janeiro: Guanabara Koogan, 2013.

KARAGEORGIU, V.; KAPLAN, D. Porosity of 3D biomaterial scaffolds and osteogenesis. **Biomaterials**, [s. l.], v. 26, n. 27, p. 5474–5491, 2005.

KELLY, J. R.; DENRY, I. Stabilized zirconia as a structural ceramic: An overview. **Dental Materials**, [s. l.], v. 24, n. 3, p. 289–298, 2008.

KHANUJA, H. S.; VAKIL, J. J.; GODDARD, M. S.; MONT, M. A. Cementless femoral fixation in total hip arthroplasty. **Journal of Bone and Joint Surgery - Series A**, [s. l.], v. 93, n. 5, p. 500–509, 2011.

KOKUBO, T.; TAKADAMA, H. How useful is SBF in predicting in vivo bone bioactivity? **Biomaterials**, [s. l.], v. 27, n. 15, p. 2907–2915, 2006.

KRISHNAN, V.; LAKSHMI, T. Bioglass: A novel biocompatible innovation. **Journal of Advanced Pharmaceutical Technology and Research**, Department of Oral Medicine and Radiology, SRM Kattankulathur Dental College and Hospitals, Chennai, India, v. 4, n. 2, p. 78–83, 2013.

L.L. HENCH, R.J. SPLINTER, W.C. ALLEN, T. K. G. Bonding

mechanism at interface of ceramic prosthetic materials. **Biomedical Materials**, [s. l.], 1972.

LACEFIELD, W. R.; HENCH, L. L. The bonding of Bioglass @ to a cobaltchromium surgical implant alloy. [s. l.], 1985.

LAURENCIN, C.; KHAN, Y.; EL-AMIN, S. Bone graft substitutes. **Expert Rev Med Devices**, [s. l.], v. 3, n. 1, p. 49–57, 2006.

LIU, X.; HUANG, A.; DING, C.; CHU, P. K. Bioactivity and cytocompatibility of zirconia (ZrO₂) films fabricated by cathodic arc deposition. **Biomaterials**, [s. l.], v. 27, n. 21, p. 3904–3911, 2006.

LIU, Y.; LIM, J.; TEOH, S. H. **Review: Development of clinically relevant scaffolds for vascularised bone tissue engineering**, 2013.

LOH, Q.; CHOONG, C. Three-dimensional scaffolds for tissue engineering applications: Role of porosity and pore size. **Tissue Eng B Rev**, [s. l.], 2013.

MA, J.; CHEN, C. Z.; WANG, D. G.; MENG, X. G.; SHI, J. Z. Influence of the sintering temperature on the structural feature and bioactivity of sol-gel derived SiO₂-CaO-P₂O₅ bioglass. **Ceramics International**, [s. l.], v. 36, n. 6, p. 1911–1916, 2010.

MA, P. X. Scaffolds for tissue fabrication. **Mater Today**, [s. l.], v. 7, p. 30–40, 2004. a.

MA, P. X. Scaffolds for tissue fabrication. **Materials Today**, [s. l.], v. 7, n. 5, p. 30–40, 2004. b. Disponível em: <[http://dx.doi.org/10.1016/S1369-7021\(04\)00233-0](http://dx.doi.org/10.1016/S1369-7021(04)00233-0)>

MAÇON, A. L. B.; KIM, T. B.; VALLIANT, E. M.; GOETSCHUIS, K.; BROW, R. K.; DAY, D. E.; HOPPE, A.; BOCCACCINI, A. R.; KIM, I. Y.; OHTSUKI, C.; KOKUBO, T.; OSAKA, A.; VALLET-REGÍ, M.; ARCOS, D.; FRAILE, L.; SALINAS, A. J.; TEIXEIRA, A. V.; VUEVA, Y.; ALMEIDA, R. M.; MIOLA, M.; VITALE-BROVARONE, C.; VERNÉ, E.; HÖLAND, W.; JONES, J. R. A unified in vitro evaluation for apatite-forming ability of bioactive glasses and their variants. **Journal of Materials Science: Materials in Medicine**, [s. l.], v. 26, n. 2, p. 1–10, 2015.

MARIEB, E. N.; WILHELM, P. B.; MALLATT, J. **Anatomia Humana Anatomia Humana**. São Paulo: Pearson Education do Brasil, 2014.

MAVROGENIS, A. F.; DIMITRIOU, R.; PARVIZI, J.; BABIS, G. C. Biology of implant osseointegration. **Journal of Musculoskeletal Neuronal Interactions**, [s. l.], v. 9, n. 2, p. 61–71, 2009.

MESQUITA-GUIMARÃES, J.; DETSCH, R.; RAMOS, L.; GRÜNEWALD, A.; HENRIQUES, B.; FREDEL, M. C.; SILVA, F. S.; BOCCACCINI, A. R. Evaluation of in vitro properties of 3D micro-macro porous bioactive hybrid scaffolds for bone grafting by human osteoblast-like cell growth. [s. l.], p. 1–38, [s.d.].

MESQUITA-GUIMARÃES, J.; LEITE, M. A.; SOUZA, J. C. M.; HENRIQUES, B.; SILVA, F. S.; HOTZA, D.; BOCCACCINI, A. R.; FREDEL, M. C. Processing and strengthening of 58S bioactive glass-infiltrated titania scaffolds. **Journal of Biomedical Materials Research - Part A**, [s. l.], v. 105, n. 2, p. 590–600, 2017.

MOHAMAD, Y. D.; BRETCANU, O.; BOCCACCINI, A. Polymer-bioceramic composites for tissue engineering scaffolds. **J Mater Sci**, [s. l.], 2008.

MONJE, A.; URBAN, I. A.; MIRON, R. J.; CABALLE-SERRANO, J.; BUSER, D.; WANG, H.-L. Morphologic Patterns of the Atrophic Posterior Maxilla and Clinical Implications for Bone Regenerative Therapy. **The International journal of periodontics & restorative dentistry**, [s. l.], v. 37, n. 5, p. e279–e289, [s.d.].

ORÉFICE, R. L.; PEREIRA, M. D. M.; MANSUR, H. S. **Biomateriais: Fundamentos e Aplicações**. Rio de Janeiro: Cultura Médica, 2006.

ÖZKURT, Z.; KAZAZOĞLU, E. Zirconia Dental Implants: A Literature Review. **Journal of Oral Implantology**, [s. l.], v. 37, n. 3, p. 367–376, 2011. Disponível em: <<http://www.joionline.org/doi/abs/10.1563/AAID-JOI-D-09-00079>>

PARITHIMARKALAINAN, S.; PADMANABHAN, T. V. Osseointegration: An update. **Journal of Indian Prosthodontist Society**, [s. l.], v. 13, n. 1, p. 2–6, 2013.

PEREIRA, R. do V. Universidade Federal de Santa Catarina Departamento de Engenharia Mecânica Programa de Pós-Graduação em Ciência e Engenharia de Materiais Projeto de Dissertação de Mestrado : Arcabouço compósito biodegradável produzido via sinterização seletiva a laser co. [s. l.], 2011.

PEREIRA, R. do V.; SALMORIA, G. V.; MOURA, M. O. C. De; ARAGONES, Á.; FREDEL, M. C. Scaffolds of PDLLA/bioglass 58S produced via selective laser sintering. **Materials Research**, [s. l.], v. 17, n. suppl 1, p. 33–38, 2014. Disponível em: <http://www.scielo.br/scielo.php?script=sci_arttext&pid=S1516-14392014000700007&lng=en&tlng=en>

PEREZ RA, M. G. Role of pore size and morphology in musculo-skeletal tissue regeneration. **Mater Sci Eng C**, [s. l.], p. 922–939, 2016.

RAHAMAN, M. N.; LIU, X.; BAL, B. S.; DAY, D. E.; BI, L.; BONEWALD, L. F. Bioactive glass in bone tissue engineering. **Ceramic Transactions**, [s. l.], v. 237, n. 6, p. 73–82, 2012. Disponível em: <<http://dx.doi.org/10.1016/j.actbio.2011.03.016>>

RAMIRO-GUTIÉRREZ, M.; WILL, J.; BOCCACCINI, A. Reticulated bioactive scaffolds with improved textural properties for bone tissue engineering: nanostructured surfaces and porosity. **Journal of biomedical materials research. Part A**, [s. l.], v. 102, n. 9, p. 2982–92, 2014.

RATNER, B. D.; HOFFMAN, A. S.; SCHOEN, F. J. and; LEMONS, J. E. **Biomaterial Science - An Introduction to Materials in Medicine**. 3. ed. [s.l.] : Elsevier, 2013. Disponível em: <<http://ilkerpolatoglu.cbu.edu.tr/docs/Introduction to Materials.pdf>>

REZWAN, K.; CHEN, Q.; BLAKER, J.; BOCCACCINI, A. Biodegradable and bioactive porous polymer/inorganic composite scaffolds for bone tissue engineering. **Biomaterials**, [s. l.], 2006.

ROLDÁN, J. C.; SCHULZ, P.; KLÜNTER, T.; DEISINGER, U.; DIEZ, C.; WAISS, W.; KIRSCHNECK, C.; REICHERT, T. E.; DETSCH, R. BMP-7 preserves surface integrity of degradableceramic cranioplasty in a Göttingen minipig model. **Plastic and Reconstructive Surgery - Global Open**, [s. l.], v. 5, n. 3, p. 1–11, 2017.

SAIZ, E.; ZIMMERMANN, E. A.; LEE, J. S.; WEGST, U. G. K.; TOMSIA, A. P. Perspectives on the role of nanotechnology in bone tissue engineering. **Dental Materials**, [s. l.], v. 29, n. 1, p. 103–115, 2013. Disponível em: <<http://dx.doi.org/10.1016/j.dental.2012.08.001>>

SANTOS, H. E. S. Propriedades mecânicas da zircônia tetragonal policristalina estabilizada por ítria submetida à degradação hidrotérmica. [s. l.], p. 139, 2012.

SANTOS, L. A. **Desenvolvimento de fosfato de cálcio reforçado por fibras para uso na área médico-odontológica**. 2002. Universidade Estadual de Campinas, [s. l.], 2002.

SANTOS, R. L. P.; SILVA, F. S.; NASCIMENTO, R. M.; MOTTA, F. V.; SOUZA, J. C. M.; HENRIQUES, B. On the mechanical properties and microstructure of zirconia-reinforced feldspar-based porcelain. **Ceramics International**, [s. l.], v. 42, n. 12, p. 14214–14221, 2016.

SCHUBERT, H. Anisotropic Thermal Expansion Coefficients of Y2O3-Stabilized Tetragonal Zirconia. **Journal of the American Ceramic Society**, [s. l.], v. 69, n. 3, p. 270–271, 1986.

SCHÜNEMANN, F. H.; GALÁRRAGA-VINUEZA, M. E.; MAGINI, R.; FREDEL, M.; SILVA, F.; SOUZA, J. C. M.; ZHANG, Y.; HENRIQUES, B. Zirconia surface modifications for implant dentistry. **Materials Science and Engineering: C**, [s. l.], v. 98, p. 1294–1305, 2019.

SEBDANI, M. M.; FATHI, M. H. Fabrication and Characterization of Hydroxyapatite-Forsterite-Bioactive Glass Composite Nanopowder for Biomedical Applications. **International Journal of Applied Ceramic Technology**, [s. l.], v. 8, n. 3, p. 553–559, 2011. Disponível em: <<http://doi.wiley.com/10.1111/j.1744-7402.2010.02601.x>>

SEPULVEDA, P.; JONES, J. R.; HENCH, L. L. Characterization of melt-derived 45S5 and sol-gel-derived 58S bioactive glasses. **Biomed Mater Res**, [s. l.], v. 58, 2001.

SEPULVEDA, P.; JONES, J. R.; HENCH, L. L. In vitro dissolution of melt-derived 45S5 and sol-gel derived 58S bioactive glasses. **Journal of Biomedical Materials Research**, [s. l.], 2002. a.

SEPULVEDA, P.; JONES, J. R.; HENCH, L. L. In vitro dissolution of melt-derived 45S5 and sol-gel derived 58S bioactive glasses. **Journal of Biomedical Materials Research**, [s. l.], v. 61, n. 2, p. 301–311, 2002. b.

SHADJOU, N.; HASANZADEH, M. Bone tissue engineering using silica-based mesoporous nanobiomaterials:Recent progress. **Materials Science and Engineering C**, [s. l.], v. 55, p. 401–409, 2015. Disponível em: <<http://dx.doi.org/10.1016/j.msec.2015.05.027>>

SHADJOU N, H. M. Bone tissue engineering using silica- based mesoporous nanobiomaterials: Recent progress. **Mater Sci Eng C**, [s. l.], 2015.

SOUZA, J.; GALARRAGA-VINUEZA, M. E.; HENRIQUES, B.; HOTZA, D.; BOCCACCINI, A. R. Current state of nanostructured biomaterials for oral and cranio-maxillofacial rehabilitation. In: **Nanostructured biomaterials for cranio-maxillofacial and oral applications**. [s.l.] : Elsevier Sci Ltd, 2018.

SRIVASTAVA, A. K.; PYARE, R.; SING, S. P. Elastic Properties of substituted 45S5 Bioactive Glasses and Glass - ceramic. **Int J Scientific Engineering Res**, [s. l.], 2012.

STANDRING, S.; WIGLEY, C.; COLLINS, P.; WILLIAMS, A.; CODY, F.; ROWLERSON, A. **Gray's Anatomy**. 39. ed. [s.l.] : Elsevier, 2008.

TIAINEN, H.; LYNGSTADAAS, S.; ELLINGSEN, J.; HAUGEN, H. Ultra-porous titanium oxide scaffold with high compressive strength. **J Mater Sci Mater Med**, [s. l.], 2010.

WANG, H.; LI, Y.; ZUO, Y.; LI, J.; MA, S.; CHENG, L. Biocompatibility and osteogenesis of biomimetic nano-hydroxyapatite/polyamide composite scaffolds for bone tissue engineering. **Biomaterials**, [s. l.], v. 28, p. 3338–3348, 2007.

WHEELER, D. L.; STOKES, K. E.; HOELLRICH, R. G.; CHAMBERLAND, D. L.; MCLOUGHLIN, S. W. Effect of bioactive glass particle size on osseous regeneration of cancellous defects. **Journal of biomedical materials research**, [s. l.], v. 41, n. 4, p. 527–

33, 1998.

XIA, W.; CHANG, J. Bioactive glass scaffold with similar structure and mechanical properties of cancellous bone. **Journal of Biomedical Materials Research - Part B Applied Biomaterials**, [s. l.], 2010.

ZHANG, Y.; LEGEROS, R.; KIM, J.-W. **Bioactive Graded Zirconia-Based Structures**, US8703294B2, 2014.

ZHONG, J.; GREENSPAN, D. C. Processing and properties of sol-gel bioactive glasses. **J Biomed Mater Res**, [s. l.], v. 53, 2000.